Journal of Power Sources 195 (2010) 1271–1291

Contents lists available at ScienceDirect

Journal of Power Sources

journal homepage: www.elsevier.com/locate/jpowsour

Review

A review on air cathodes for zinc–air fuel cells

Vladimir Neburchilov, Haijiang Wang*, Jonathan J. Martin, Wei Qu

Institute for Fuel Cell Innovation, National Research Council Canada, 4250 Wesbrook Mall, Vancouver, BC, Canada V6T 1W5

ARTICLE INFO

Article history:
Received 23 June 2009
Received in revised form 29 August 2009
Accepted 31 August 2009
Available online 19 September 2009

Keywords:
ZAFC
Air cathode
Bifunctional electrode
Oxygen reduction reaction
Synthesis
Cathode design
Mechanically recharged metal–air battery
Secondary metal–air battery

ABSTRACT

This paper reviews the compositions, design and methods of fabrication of air cathodes for alkali zinc–air fuel cells (ZAFCs), one of the few successfully commercialized fuel cells. The more promising compositions for air cathodes are based on individual oxides, or mixtures of such, with a spinel, perovskite, or pyrochlore structure: MnO_2, Ag, Co_3O_4, La_2O_3, $LaNiO_3$, $NiCo_2O_4$, $LaMnO_3$, $LaNiO_3$, etc. These compositions provide the optimal balance of ORR activity and chemical stability in an alkali electrolyte. The sol–gel and reverse micelle methods supply the most uniform distribution of the catalyst on carbon and the highest catalyst BET surface area. It is shown that the design of the air cathode, including types of carbon black, binding agents, current collectors, Teflon membranes, thermal treatment of the GDL, and catalyst layers, has a strong effect on performance.

Contents

* Corresponding author. Tel.: +1 604 221 3038; fax: +1 604 221 3001.
E-mail address: haijiang.wang@nrc.gc.ca (H. Wang).

0378-7753/$ – see front matter.
doi:10.1016/j.jpowsour.2009.08.100

0. Introduction

In 1868, Leclanche developed the first metal–air battery with a MnO_2/carbon cathode electrode, leading the way for Heise and Schudmacher to develop a more modern design in 1932 [1]. Metal–air fuel cells, also called air-depolarized batteries, consist of a metal anode (negative) and an oxygen cathode (positive). Zinc–air fuel cells (ZAFCs) are one of the more mature metal–air fuel cell technologies [2–13]. ZAFCs differ from zinc–air batteries by fuel refuelling. Non-rechargeable ZAFCs are known as primary ZAFCs and rechargeable ZAFCs are known as secondary ZAFCs [14,15]. The typical ZAFC design is given in Fig. 1 [16].

Typical ZAFCs are comprised of an alkali electrolyte, a replaceable supply of Zn at the anode, an air cathode, which usually consists of a non-precious metal catalyst, and a polymer separator. The ZAFCs require refuelling with new alkali electrolyte and Zn supply as well as the removal of reaction products such as zinc oxide and potassium zincates.

The recharging/recycling process of the ZAFCs includes [17]:

1. Disassembly of the used Zn source (typically 80% Zn utilization).
2. Reaction of the Zn anode oxidation product (ZnO) with the electrolyte (KOH):

$$ZnO + 2KOH + 2H_2O = K_2Zn(OH)_4 \quad (1)$$

3. Electrowinning of the zincate solution:

$$K_2Zn(OH)_4 = Zn + 2KOH + H_2O + (1/2)O_2 \quad (2)$$

4. Reassembly of the Zn source containing the electrowinned Zn.

In comparison with proton exchange membrane fuel cells (PEMFCs), commercialization of ZAFCs have begun for applications such as stationary generators by Power Air Corp. (USA), electrical buses and scooters by Powerzinc Electric Inc. (China), and hearing aids (zinc–air batteries). The main advantages of ZAFCs vs. batteries are: high specific energy (200 Wh kg^{-1}, 225 Wh L^{-1}) [7], fuel recycling, the ability to refuel quickly, low cost, and unrestricted outdoor siting. The main advantages of ZAFCs vs. PEMFCs are: cost-effective design (non-precious catalysts, cheap zinc recovery equipment and absence of expensive membranes, bipolar plates and hydrogen sensors), non-hazardous fuel storage, low maintenance costs, and technology that is closer to commercialization. Lastly, the market for ZAFCs was evaluated to be $251.1 million [18], which consists of: hearing aids, back-up power devices, stationary and portable home power generators, mobile electronic devices (PDA, cell phones, laptop, etc.), and hybrid electric vehicles (HEV) or electric vehicles (EVs) [19–21].

The growth of the industry shown in the forecast [18] is due to the increasing environmental considerations for batteries in mass production products such as automobiles and portable electronics. Hearing aids, currently the largest segment of the ZAFC market, have already achieved market saturation (mature stage of a technological cycle).

The button metal–air fuel cell design is common for portable electronic applications. While these fuel cells began to be actively developed 40 years ago, in the early 1970s ZAFCs were prone to leakage. By the mid-1970s, design led to the successful introduction of zinc–air button batteries for use in hearing aids as a replacement for 2-electrode cells. By the mid 1980s, zinc–air batteries had become the standard for hearing aid applications. Since that time, button batteries have seen significant development towards ZAFCs with increased electrochemical capacity, cell-to-cell performance consistency, and control of electrolyte leakage, while providing a higher voltage and limiting current and controlling movement of

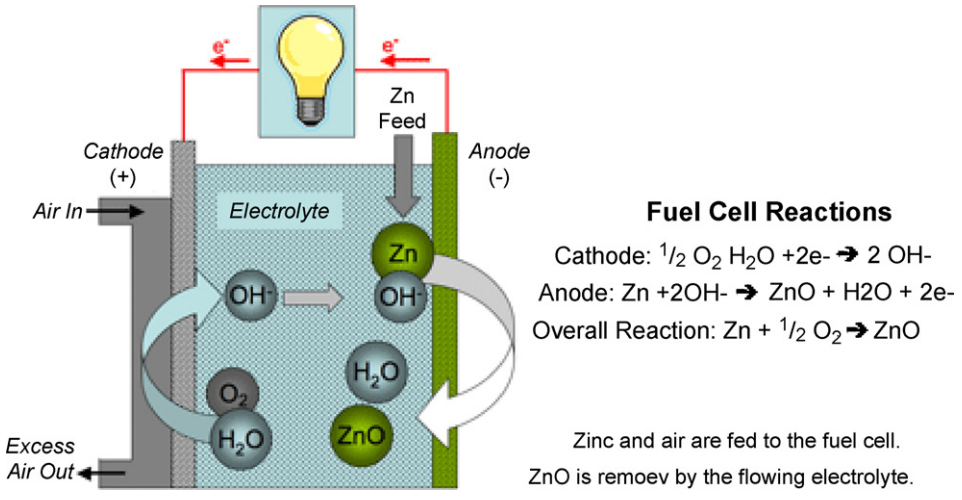

Fig. 1. Design of typical ZAFC [16].

moisture into and out of the cell [22]. Lawrence Livermore National Laboratory (LLNL) developed secondary, rechargeable, ZAFCs for other applications, including vehicles with a range of 250–350 miles before refuelling [23].

Rechargeable ZAFCs include two main designs that utilize either two or three electrodes [1,6]. The three-electrode design consists of two separate electrodes for the oxygen reduction reaction (ORR) and oxygen evolution reaction (OER). In this cell, the zinc electrode is located between the air cathode and a third electrode for the OER. The air cathode is electrically isolated during the charging process, which increases its lifetime by avoiding exposure to the high OER potential. The electrolyte enclosed between the air cathode and the porous substrate for zinc deposition contains zincate ions, whereas the electrolyte between the third electrode and the zinc electrode is zincate free. The Zn produced during charging of the three-electrode cell is deposited on the portion of the support facing the air cathode. Conversely, the two-electrode design consists of a zinc electrode and a bifunctional air electrode having active catalytic components for both the OER during the charge cycle and the ORR during the discharge cycle. Since the air electrode can work as cathode for ORR and anode for OER, this simple design does not require separation of the two electrolyte flows.

The air cathode of ZAFCs is one of the most expensive cell components and is largely responsible for determining the performance of the fuel cell. The air cathode of Alupower Ltd., for example, has a price of \$120 m^{-2} and an energy cost of \$50 kW^{-1} at a high surface power density of 5 kW m^{-2} with the cathode catalyst responsible for 50% of this cost [23]. The growth in demand for cost-effective non-noble air cathodes has increased activity in the development of novel ORR catalysts that are active and durable in alkaline electrolytes.

1. Air cathode compositions

The oxygen reduction reaction in aqueous solutions can proceed by two pathways: a direct four-electron pathway and a peroxide two-electron pathway. In the direct four-electron pathway, oxygen directly reduces to OH^-. In the peroxide two-electron pathway, an initial reduction to HO_2^- is followed by the reduction of HO_2^- to OH^- [24]. The peroxide pathway of the ORR is more common in alkaline solutions and the direct four-electron pathway of the ORR proceeds by dissociative absorption on the metal catalyst surface.

1.1. MnO_2-based ORR catalysts

The first ZAFCs, built by Leclanche, had a MnO_2-based air cathode to reduce the parasitic effect of peroxide generation in metal–air cells. It has been proposed that manganese oxides have high catalytic activity for the decomposition of H_2O_2 because the decomposition is based on the simultaneous oxidation and reduction of the surface manganese ions [25,26] (i.e., Mn^{4+}/Mn^{3+} for the mixed manganese based catalyst [27]). Mao et al. [28] established that the presence of MnO_x, including Mn_2O_3, Mn_3O_4, Mn_5O_8 and MnOOH, on Nafion-modified Au electrodes enhanced the first reduction current peak of O_2 to HO_2^- and decreased the second peak of HO_2^- to OH^- without a potential shift. MnOx also promoted oxygen disproportionation and resulted in an overall four-electron reduction of O_2 on MnOx/Nafion-modified Au electrodes. Currently, it is also a popular ORR catalyst for ZAFCs.

The majority of the ZAFC air cathode patents analyzed in this review are based on manganese oxide [28–57] and the general design of these cathodes is given in Table 1. In recent years, significant progress has been made in the improvement of the durability and ORR activity of these carbon supported air cathodes. Yang and Xi [56] identified the ORR pathway for nanoporous amorphous manganese oxide as the two-electron process (load 0.85 mg cm^{-2}). In a three-electrode cell, it demonstrated a higher current density ($j > 100$ mA cm^{-2}) with an oxygen back-feed than with nitrogen in 1 M KOH (Fig. 2). The catalyst was produced by reacting sodium permanganate with disodium fumarate and the high ORR activity was explained by the high concentration of lattice defects and active sites in the amorphous material $Na_{0.10}MnO_{1.96}{\cdot}0.7H_2O$. The mean oxidation state of manganese was determined to be 3.82.

Table 1
Design of MnO_2-based air cathode.

Number	Component
1	Microporous Teflon membrane with high air permeability. It limits the maximum ZAFC current to 100 mA cm^{-2}
2	Current collector
3	Gas diffusion layer.
4	Catalyst layer (MnO_2)

Table 2
Effect of heat treatment temperature on the stability of 10% CoTMPP/C air cathodes in 7 M KOH at $j = 100$ mA cm^{-2} [89].

Temperature, °C		460	610	730	810
Initial potential, mV vs. Hg/HgO		120	120	120	120
Potential, mV vs. Hg/HgO, after test	2500 h	300	~220	~180	~170
	4000 h	–	–	~225	~210

Due to different morphologies and surface states, the properties of MnO_2 are influenced by the method of fabrication [57], which includes both chemical and electrochemical methods. The chemical methods include the heating of manganese nitrate [28–30] and the reduction and heating of $KMnO_4$ [31–34]. Zoltowski et al. [49] disclosed the use of potassium permanganate to catalyze activated carbon, wherein most of the permanganate was reduced to MnO_2 by the carbon. Armstrong et al. [32] disclosed a similar admixture of potassium permanganate and activated carbon, wherein the potassium permanganate was reduced in situ, by either heating or the introduction of hydrogen peroxide, to form MnO_2. Bach et al. [33] disclosed the sintering of potassium permanganate at 250–700 °C in an oxidizing atmosphere, which produced a mixture of the oxides MnO_2, Mn_2O_3, and Mn_3O_4. Hoge et al. [34,35] used the potassium permanganate as the catalyst for a carbon supported air cathode. The Mn(II) isopropoxide has also been used as the catalyst for an air cathode and the design of an air cathode utilizing a MnO_2-based catalyst is given in Table 2 [36].

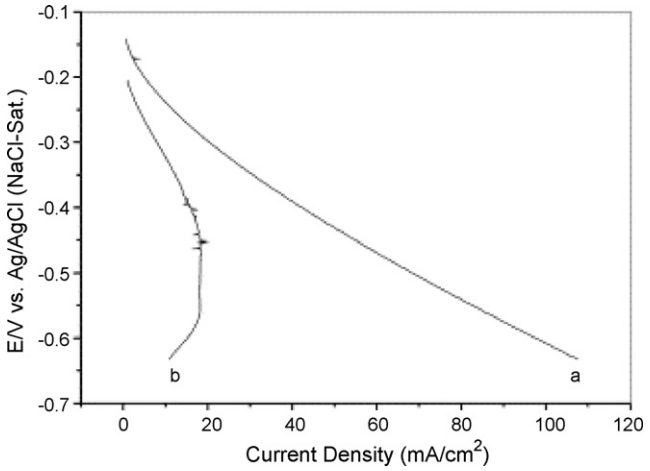

Fig. 2. ORR polarization curves of a catalytic electrode based on amorphous manganese oxide in a gas diffusion electrode setup with: (a) oxygen and (b) nitrogen as the back-feed [56].

Air Energy Resources Inc. (AER) also used the Mn(II) precursor isopropoxide, but they utilized the more advanced sol–gel method for fabrication. The air cathode composition of 5% MnO_2 + 75% C (a mixture of 30% Ketjen Carbon Black EC-600JD (EC-600JD) from AKZO with a BET surface area of 1200 $m^2\,g^{-1}$ and 70% AB50 Shawinigan carbon black (AB-50) from Chevron with a BET surface area of 70–90 $m^2\,g^{-1}$) + 20% PTFE [37] employs a novel approach for water management in the coating by combining two carbon blacks with low and high BET surface area. This approach leads to an optimum balance of hydrophobic/hydrophilic properties and allows for good oxygen adsorption. Sol was formed by the addition of water to an alcoxide/alcohol solution. Gel was produced by heat treatment and evaporation of the alcohol. The pyrolysis of the gel and active carbon mixture in air at T = 150–250 °C produces the final composition. AER used the micelle method and combined active carbon and carbon black for additional improvement of the air cathode: 5% MnO_2 (Mn^{3+}/Mn^{4+}) + 70% C (60% active Calgon Carbon PWA + 40% carbon black) + 25% PTFE (Teflon 30B). Design of the GDL layer was also improved through addition of low and high BET carbon blacks (30% EC-600JD + 70% AB-50). This company also utilized another micelle encapsulation method, for the fabrication of MnO_x-based catalysts [38]:

1 Prepare the 1st solution: 60% Cyclohexane (solvent) + 25.5% Igepal 520 (surfactant) + 25% $Mn(NO_3)_2$.
2 Prepare the 2nd solution: 60% Cyclohexane (solvent) + 25.5% Igepal (surfactant) + 15% tetraethylammonium hydroxide $(C_2H_5)_4NOH$.
3 Sonicate the mixture of the 1st and 2nd solutions.
4 Add 19 g of active iodine carbon Calgon PWA per 1 g of Mn and sonicate for 30 min.
5 Centrifugation and deposition.
6 Heat in inert gas at 500 °C, 2 h, Mn-MnO_2.
7 Add the 30% EC-600JD + 70% AB-50 mixture.
8 Add 20 wt.% Teflon.
9 Dry at 100 °C for 20 h
10 Chop catalyst in a blender for 180 μm particles

Dry pressing was employed to coat the current collector with the prepared catalysts and GDL powders.

Ndzebet designed an air cathode with a combination of high and low BET surface carbon blacks with the following composition [39]: MnO_2 + C (activated carbon, BET—900 $m^2\,g^{-1}$ + Carbon Black Pearls 2000 carbon black (BP2000) from Cabot, BET—1500 $m^2\,g^{-1}$) + PTFE. The particle size distribution of the MnO_2 catalyst was established to be 20–26 μm. A performance test in 30% KOH achieved a potential of 1.15 V at 150 mA cm^{-2} (over 15 h).

Koshiba et al. [40] obtained a limiting current of 11 mA cm^{-2} (compared to commercial catalysts at 50–100 mA cm^{-2}) with a ZAFC air cathode composed of 30% MnO_2 + 20% activated carbon + 20% carbon black + 30% PTFE. The MnO_2 was produced by heat treatment of γ-manganese oxy-hydroxide at 250–450 °C with the decomposition products of Mn_5O_8 + β-MnO_2. This patent used the combination of the activated carbon and carbon black (30% MnO_2 + 20% active carbon + 20% carbon black + 30% PTFE) to improve performance.

Sun et al. [42] used catalyst with 20% MnO_2 + 70% activated carbon + 10% PTFE with a GDL composed of 15% carbon black + 85% PTFE. After 1 h of discharging, a voltage of 1.32 V was measured at a load of 620 Ω.

The chemical fabrication methods for MnO_2 require significant time (about 130 h) and are limited to a maximum BET surface area of 400 $m^2\,g^{-1}$ to minimize the risk of spontaneous combustion. Thus, Duracell Inc. [43] used the milling of electrolytic or chemical γ-MnO_2 (EMD or CMD, respectively) for the air cathode (11% γ-MnO_2 + 41% BP2000 + 48% PTFE). The ZAFC with this cathode had a 430 mAh capacity when 1.0 V was used as the cutoff voltage. The other Duracell cathode composition [44] of MnO_2 + PTFE + 2–20% absorbent (gelling material) was used in the air cathode, giving a limiting current of 27.5 mA at T = 66 °C.

It was discovered that another manganese compound, MnOOH, had higher ORR activity than oxides such as Mn_2O_3, Mn_3O_4, and Mn_5O_8 in 0.1 M KOH electrolyte, due to an increased number of active centers [57]. Mn_3O_4 and γ-MnOOH were prepared by chemically oxidizing $MnSO_4$ with H_2O_2. The compounds α-Mn_2O_3 and Mn_5O_8 were made by thermally oxidizing Mn_3O_4 under an O_2-gas atmosphere at 1173 and 703 K, respectively. The best air cathode, 28.5% (9% MnO_x + 1% Ni)/C (catalyst #5 in Table 2), has a specific current density of 43.8 μA cm^{-2}, which is about 1.5 times higher than MnO_x/C (catalyst #4 in Table 2). The measurements of ORR Tafel slopes and mass activities (MA) were carried out at E = 0 V (NHE) in O_2 saturated 1 M KOH and T = 25 °C (Table 2) [47]. The measurements of ORR Tafel slopes and MA were carried out at E = 0 V (NHE). The best air cathode, MnO_x + Ni/C, has a SA of 43.8 μA cm^{-2}, which is 1.5 times higher than MnO_x/C and a 37–51 nm particle size.

1.2. Ag-based ORR catalysts

Silver has been demonstrated to be an active component for the ORR in alkaline solutions [58–70]. Wu et al. investigated silver ORR catalyst supported on carbon nanocapsules (CNC) [60]. This catalyst was produced by a simple method that combined precipitation of AgCl and reduction to Ag in a hydrogen atmosphere. The CNC (333 $m^2\,g^{-1}$, 15–30 nm) surpassed the ORR activity of Vulcan XC-72 carbon black (XC-72) from Cabot. High performance was demonstrated (j = 200 mA cm^{-2} at E = 0.8 V) resulting from dense packing that was possible due to the uniform size and the higher conductivity (30% KOH, T = 25 °C). As shown in Fig. 3, the Ag/CNC catalyst demonstrated better performance (E = 0.99 V at 200 mA cm^{-2}) than the commercially available Mn and MnCo-catalyzed air cathodes. The galvanostatic discharge for Ag/CNC at j = 200 mA cm^{-2} showed a moderate decrease in performance after 80 h. Yang and Zhou [61] also established relatively good stability and insignificant voltage deterioration of Ag on Ni foam during a 120 h galvanostatic discharge at T = 40 °C.

Expensive platinum, was found to have the highest ORR activity, however, it was insufficiently stable in alkaline electrolytes [63]. The ORR activity and stability of Pd, Ir, Co, Ru, and Ni-based electrodes (thermal method of fabrication) were investigated as well.

Ag-based air cathode improvement was achieved through doping with tungsten carbide (W_2C), which allowed for a more

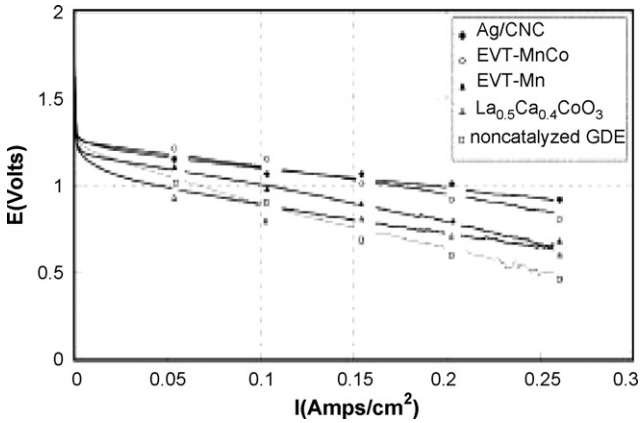

Fig. 3. The polarization curves of non-catalyzed GDE's and catalyzed GDE's with electrocatalysts of CNC, XC72, and vapour growth carbon fiber (VGCF) from Shoka Denko, Corp. All catalyst loadings were 2.52 mg cm^{-2} [60].

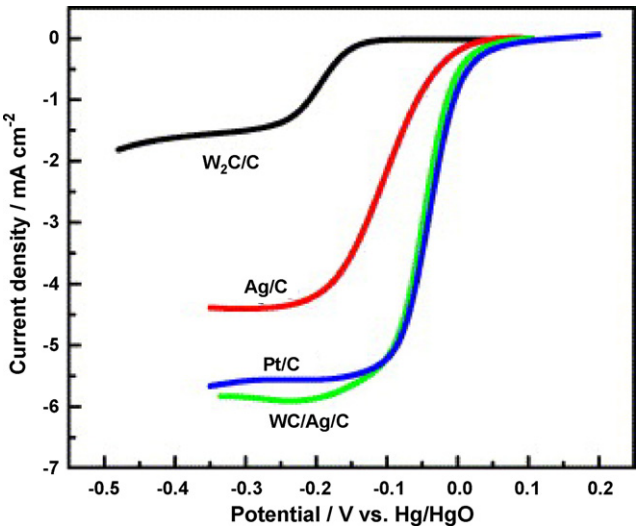

Fig. 4. Comparison of the polarization curves for the ORR on W_2C/C, Ag/C, Ag-W_2C/C and Pt/C on glassy carbon rotating disk electrodes in an O_2 saturated 1 M KOH solution (conditions: temperature—25 °C, sweep rate—5 mV s^{-1}, rotation rate—2500 rpm). Curves: W_2C/C (11.43 μg W_2C), Ag/C (11.43 μg Ag), Ag-W_2C/C (11.43 μg W_2C + 11.43 μg Ag) and Pt/C (22.86 μg Pt) [64].

promising composition for ORR in ZAFC, AgW_2C/C [64]. A comparison of the ORR activity of W_2C/C and Ag/C (Fig. 4) confirms the synergetic effect of the W_2C additive on Ag. This catalyst was produced by the intermittent microwave method (IMH). $AgNO_3$ was mixed with H_2O_2, IPA and W_2C/C in the ratio, W_2C:Ag = 1:1 before IMH treatment. Considering the porous character of the Ag coating, silver-coated WC particles are an alternative for AgWC/C worth evaluating [65].

Gillette Corporation [66] developed a new advanced catalyst consisting of 5% $AgMnO_4 + MnO_2$, based on the high stability of MnO_x in alkaline solution and its high activity for H_2O_2 decomposition. The dual catalyst ($AgMnO_4$) was prepared by reducing silver permanganate. MnO_2 was prepared by reducing $KMnO_4$ with hydrazine or by heating $Mn(NO_3)_2$. Testing of $AgMnO_4$ + (5% or 10%) MnO_2 air cathodes in a three-electrode cell demonstrated performances of 28 and 50 mA cm, respectively, at E = 0.16 V (SHE). The limiting current (51 mA cm^{-2}) occurred at E = 0.25 V (Hg/HgO) or 1.1 V (vs. Zn). Another useful approach described in the patent involved the utilization of varying Teflon concentrations in the GDL and catalyst layer depending on the purpose of the layer:

- High (30–70%) PTFE content in the GDL to prevent the cathode from wetting through.
- Low (10–30%) PTFE content in the catalyst layer to promote optimal wetting of the catalyst layer.

A catalyst consisting of a combination of silver and Raney alloy (Ni–Al) was suggested by Goldstein et al. [67]. The design of this cathode includes the GDL (C + PTFE, with a carbon loading of 6–10 mg cm^{-2}), which was pressed onto a Ni foam current collector and the catalyst layer (Ni–Al + Ag + PTFE = 5:1 wt.%) at a loading of 24 mgMe cm^{-2}). Catalyst testing showed a peak current of 10 A at E = 0.9 V during 5 h of cell discharge (a peak current of 200 mA cm^{-2} at the air cathode).

Zhong [68] used silver oxide as the ORR active component in the development of catalyst composed of Ag_2O + 10% $LaNiO_3$ (lanthanum nickelate). Performance degradation of the ZAFC was not observed during 500 h of testing in 32% KOH. Alupower, Inc. suggested a catalyst containing 5% Ag + 15% BP2000 + 10% Daxad (sodium salt of polymerized naphthalene sulphuric acid) + 60% Teflon RPM T-30. The Daxad additive was used to increase the silver adsorption on the carbon black [69].

Basically, carbon supported Ag catalysts show high ORR activity as a result of its activity for decomposition of H_2O_2, which would otherwise accumulate during the two-electron ORR pathway on carbon [62].

1.3. Mixed valence CoO_x-MnO_x ORR catalysts

Cobalt oxides were also identified as active catalysts for the ORR in alkaline solutions. Ovshinsky et al. [71] suggested novel multifunctional air cathode compositions with mixed valence components (5% (2.5–7.5%) MnO_x + 5% (2.5–7.5%) CoO_x/C and 15% CoO_x + 5% MnO_x/C, 20% CoTMPP + 15% CoO_x + 5% MnO_x). CoO_x was utilized because it has Co^{3+} ions located on the octahedral lattice sites and Co^{2+} on the tetrahedral sites. These catalysts were developed with a ratio of high and low valences in the range of 1:2 to 2:3, where the two components of the catalyst (Co^{3+} and Co^{2+}) were responsible for the two activation steps of the ORR:

- The first is for the two-electron stage of the peroxyl ion formation:

$$O_2 + H_2O + 2e = H_2O^- + OH^- \quad (3)$$

- The second for the two-electron stage of peroxyl ion decomposition:

$$H_2O^- + 2e + H_2O = 3HO^- \quad (4)$$

As the pores of this catalyst are not through-holes, the peroxide, formed during the two-electron pathway of ORR, can only diffuse into the bulk solution. During this slow diffusion, the peroxide oxidizes the Teflon bonding between the catalyst particles, carbon and other catalyst components. This decomposition, the main cause of ZAFC degradation, blocked the internal space of the pores, increased the resistance and reduced the active surface area of the ORR catalyst.

The performances of CoO_x/C, MnO_x/C, and $MnO_x + CoO_x$/C in an alkaline solution are shown in Fig. 5. The catalyst composed of 2.5% MnO_x + 7.5% CoO_x/C showed the highest ORR activity (120 mA cm^{-2} at E = −0.1 V). The fabrication procedure for the 5% CoO_x/C catalyst consisted of mixing NH_4OH and carbon in an ultrasonic bath before adding an aqueous solution of $CoSO_4$. The final solution was then treated with NaOH, which resulted in the formation of the catalyst deposit. The procedure for the preparation of the catalyst with 20% CoTMPP/C was similar.

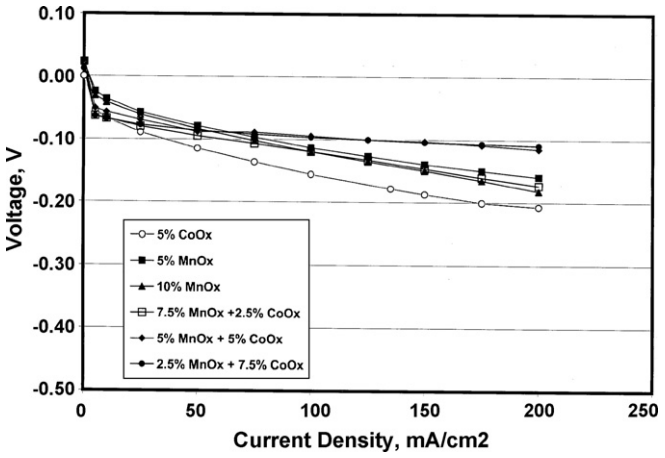

Fig. 5. Polarization curves for $CoO_x + MnO_x$ ORR catalyst in alkaline electrolyte [71].

1.4. Metal tetra-methoxylphenyl porphyrine-based ORR catalysts (CoTMPP, FeTMPP-Cl/C)

The carbon supported pyrolyzed macrocycles show good ORR activity in alkali electrolytes and are currently used in mechanically rechargeable metal–air batteries [71–78]. One popular non-noble air cathode is based on cobalt and iron tetra-methoxylphenyl porphyrine (CoTMPP and FeTMPP) [71,76–78].

CoTMPP has higher electrochemical stability and promotes the two-electron ORR pathway, while FETPP has inferior ORR activity and promotes direct four-electron oxidation. The stability of the metal macrocyclic complex depends on the metal and it decreases accordingly: Co > Fe > Mn [79]. One common approach to combine the advantages of a more stable CoTMPP and a more ORR active FeTMPP is to fabricate a mixture, FeTMPP/CoTMPP [79]. The ORR activity increases due to the formation of a face-to-face structure, accelerating the destruction of the O–O bond in the oxygen molecule [82–85]. The effect of heat treatment on increasing the stability of N_4-chelates, discovered by Jahnke et al. [86] in 1976, is currently a very popular method for the increasing the stability of Co/FeTMPP-based catalysts.

1.4.1. FeTMMP-Cl-based ORR catalysts

Gojkovic et al. [76–87] established that pyrolized FeTMMP-Cl catalyst, heat treated at $T < 200\,^{\circ}C$, has the Fe^{3+}/Fe^{2+} redox peak for CV curves in alkaline (1 M NaOH at 25 °C) and acidic solutions. This macrocyclic complex decomposes at $T > 700\,^{\circ}C$. The increase in ORR activity for the catalyst after heat treatment corresponds to the decrease in activation energy for the ORR (RRDE, 0.1 M H_2SO_4). The number of electrons exchanged per oxygen molecule (3.45–4) depends on the potential, but not the pyrolysis temperature. At low pyrolysis temperatures, the ORR on FeTMMP-Cl proceeds by the direct four-electron pathway, resulting in lower polarization [76]. The rate of the ORR on FeTMPP-Cl/BP in alkaline electrolyte is higher than in acidic solution and it is comparable with that of Pt; however, in an acidic solution, Pt is more active than FeTMMP-Cl/BP. The effect of sulfate, perchlorate and phosphate on ORR activity was not determined [87].

1.4.2. CoTMPP-based ORR catalysts

CoTMPP has higher stability in comparison to FeTMPP, which has led to its use for ZAFC air cathodes [71,77,78,88]. Iliev et al. [89] also established that the heat treatment of CoTMPP/C in argon at $T = 460–810\,^{\circ}C$ improves its ORR activity in an alkali electrolyte. The ORR activity after heat treatment at $T = 750–850\,^{\circ}C$ remains high and stable, with transport limitations increasing with time. Heat treatment of CoTMPP increases its long-term stability in both alkali [90,91] and acid [92–94] electrolytes.

The work of Mocci et al. [75] improved understanding of the ORR activity of CoTMPP in alkaline solutions. ORR activity is determined by the simultaneous presence of a metal precursor, active carbon, and a source of nitrogen. The ORR activities of pyrolized mixtures of $CoCO_3$ + TMPP + C and Co_3O_4 + CoTMPP + C (in N_2 at 800 °C) were shown to be higher than CoTMPP/C. The findings demonstrate the key role of carbon during pyrolysis, but not as a structural component for CoTMPP/C (pyrolysis in N_2 at 900 °C). Mocci and Trassatti [73] developed another interesting modification of CoTMPP—10% ($CoCO_3(Co_3O_4)$ + TMPP)/C. The choice of Co_3O_4 was based on its presence in the products of CoTMPP pyrolysis. It was established that $CoCO_3$ was the best Co-precursor for achieving maximum ORR activity for 10% ($CaCO_3(Co_3O_4)$ + TMPP)/C. The optimal fabrication method for this catalyst consists of pyrolysis of the $CoCO_3$ + TMPP or Co_3O_4 + TMPP/C mixture at 800 °C in inert gas with the addition of carbon black after heat treatment (pyrolysis at 900 °C yields catalyst with lower ORR activity). The catalyst with a molar ratio of Co/TMPP = 1:1 and weight ratio of $CoCO_3$/C = 5% demonstrated the highest ORR activity. Conversely, increasing the pyrolysis temperature for Co_3O_4 + TMMP/C fabrication decreases the Co_3O_4 surface area, which leads to a drop in ORR activity. It was shown that Co_3O_4 does not significantly improve ORR activity (it is active itself [75]) and the Co- and N-containing molecular moieties do not interact for a synergetic effect. The presence of carbon during pyrolysis more strongly effects ORR activity, as it is responsible for the partial reduction of Co_3O_4, which determines the interaction between Co ions and nitrogen moieties. The performance of 10% ($CaCO_3(Co_3O_4)$ + TMPP)/C (heat treatment at 200 °C) is higher than Co_3O_4 (0.5 and 0.1 mA cm^{-2}, respectively) at 0.3 V (SHE), 1 M KOH, and 25 °C and it is the same at $T > 600\,^{\circ}C$.

Table 3
Diameters calculated from XRD patterns after mild[a] or premature[b] ageing [47].

Catalysts	d (nm)	Mass activity, MA (A g^{-1})	Specific activity, SA (μA cm^{-2})	b (V dec^{-1})
1. MnO_x/C[a]	4	11.0	3.9	−0.062
2. Ni-MnO_x/C[a]	6	36.9	18.6	−0.059
3. Mg-MnO_x/C[a]	6	25.9	13.4	−0.044
4. MnO_x/C[b]	57	6.2	30.5	−0.098
5. Ni-MnO_x/C[b]	37	14.0	43.8	−0.074
6. Mg-MnO_x/C[b]	51	5.1	21.7	−0.074
7. 10 wt.% Pt/Vulcan XC72	2	40.1	25.8	−0.081

[a] Mild ageing of catalyst—1 year storage in ambient conditions.
[b] Premature ageing of catalyst—150 mg of each MnO_x/C powder was put into a cell with 50 ml O_2 saturated 1 M KOH at $T = 80\,^{\circ}C$ and OCP.

An air cathode consisting of 10% CoTMPP on activated carbon showed a performance of 200 mA cm^{-2} at $E = 200$ mV (Hg/HgO) in 7 M KOH at room temperature [89]. The catalyst was heat treated at $T = 460–850\,^{\circ}C$ for 5 h in Ar. A 2500 h durability test of this cathode demonstrated an increase of the initial potential of the electrodes heat treated at 460, 610, 730, 810 °C from 120 (Hg/HgO) to 300, 220, 180, and 170 mV, respectively (Table 3). Thus, the best stability for this electrode was achieved with a heat treatment at 730–810 °C (810 °C being optimal).

One method for improving the ORR activity of CoTMMP-based catalysts is through the addition of MnO_2, which is active for H_2O_2 decomposition [88]. This work was conducted in collaboration with Powerzinc Electric Inc. (Shanghai, China). The MnO_x + CoTMPP/C (BP2000) catalyst promotes the two-electron pathway of the ORR with the rate-limiting step being the formation of peroxide in 1 M KOH at $T = 25\,^{\circ}C$ (RRDE in a half-cell). The ORR activity of CoTMPP was improved through modification with MnO_x, one of the most commonly used ORR catalysts for ZAFCs [88]. Suspensions of $KMnO_4$/C and $MnSO_4$/KOH (pH 8) were mixed to produce MnO_x/C (BP 2000), as detailed by the following reaction:

$$2MnO_4^- + 3Mn^{2+} + 2H_20 = 5MnO_2 + 4H^+ \quad (5)$$

In this work carbon black, carbon nanotubes (CNT), and BP2000 were investigated as the support for CoTMPP/C catalysts. BP2000, activated by 30% H_2O_2, supplied the highest peak current for oxygen reduction. H_2O_2 oxidizes the carbon support during ORR but preliminary treatment of the carbon in H_2O_2 increases ORR activity. The tetragonal structure of Mn_2O_3 changes to cubic MnO_x at $T = 800\,^{\circ}C$, with particle sizes of 5–30 nm. At $T = 900\,^{\circ}C$, the cubic MnO_x granules become spherical. This catalyst demonstrated a performance of $j = 500$ mA cm^{-2} at $E = -0.498$ V (Hg/HgO) in a half-cell with 1 M KOH at $T = 25\,^{\circ}C$ (Fig. 6). A ZAFC with a MnO_x + CoTMPP/C air cathode (heat treatment at $T = 800\,^{\circ}C$, catalyst mass loading of 14.6 mg cm^{-2}) demonstrated a maximum output current density of 216.3 mA cm^{-2} at a 1 V output potential in 30% KOH (Fig. 7) [88].

A similar CoTMPP doping procedure with MnO_x was developed to fabricate 4% CoTMPP + 15% C (BP2000) + 60% Teflon RTM

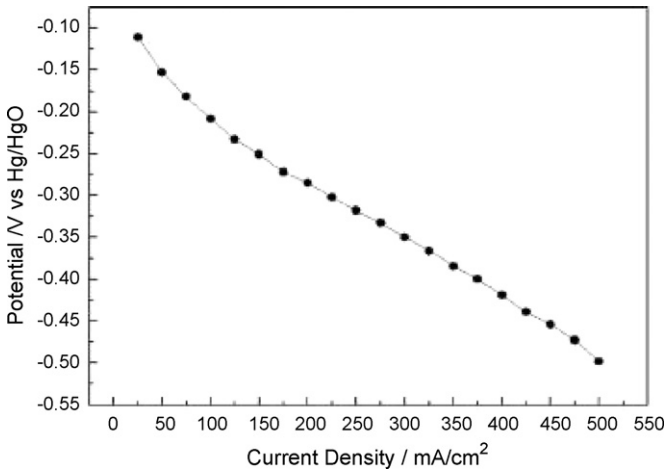

Fig. 6. ORR polarization curves for MnO_x-CoTMPP/BP catalyst with treatment of carbon black by 30% H_2O_2 in oxygen saturated 1 M KOH at $T = 20\,^{\circ}C$ in half-cell [88].

T-30 + MnO_2 (Co_3O_4) [78]. Two methods were used to prepare this CoTMPP-based electrode: a wet powder process and a dry powder process. The wet method produced a catalyst with higher performance than the dry method (discharge voltage of 1 V at 500 mA cm^{-2}, in comparison with 200 mA cm^{-2} for the dry method). After soaking the electrode in 7 M KOH at 25 °C overnight and applying a duty cycle for 1 h (20 s—200 mA cm^{-2}, 45 s—50 mA cm^{-2}, 45 s—0 mA cm^{-2}), the voltage was $E = -0.29$ V (Hg/HgO) at $j = 0.4$ A cm^{-2}. This performance was stable during 200 h of testing.

CoTMPP air cathodes demonstrate high stability in not only ZAFC conditions, but also in hot alkaline electrolyte. The developed air cathode [10% CoTMPP + 90% Carbon (Shawinigan)] + Nafion shows good performance at a current density of 450 mA cm^{-2} (an initial voltage of 0.53 V (SHE), 0.77 V after 3 h, and 0.54 V after 134 days) [95].

Another interesting approach for improving the ORR activity of CoTMPP-based catalysts was through doping with CoO_x (Fig. 8) [71]. Catalysts with compositions consisting of 1–5%[50% (20% CoTMPP/C) + 50% (15% CoO_x + 5% MnO_x)]/C and 1–5%[7.5% CoO_x + 2.5% MnO_x]/C have a performance of $E = -0.09$ and -0.11 V, respectively, at of $j = 200$ mA cm^{-2} and are shown in Fig. 8. The properties of CoTMPP and methods of CoTMPP-based ORR catalyst fabrication are given in [80,96].

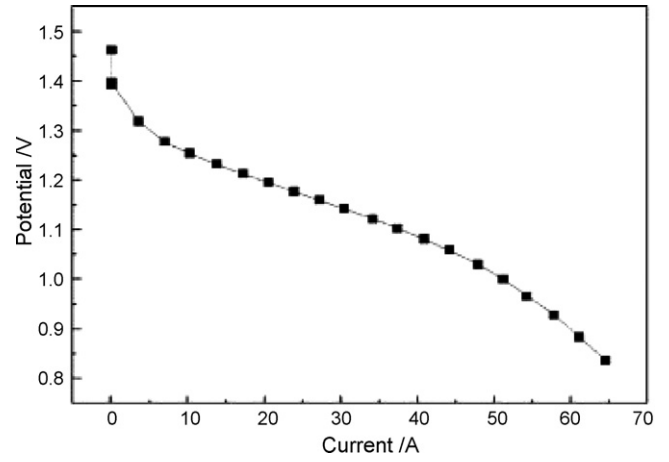

Fig. 7. Current–potential curve of a zinc–air cell based on a MnO_x-CoTMPP/C (BP2000) air cathode (the BP2000 was treated with 30% H_2O_2) and a Zn counter electrode with an active electrode surface area of 236.8 cm^2 [88].

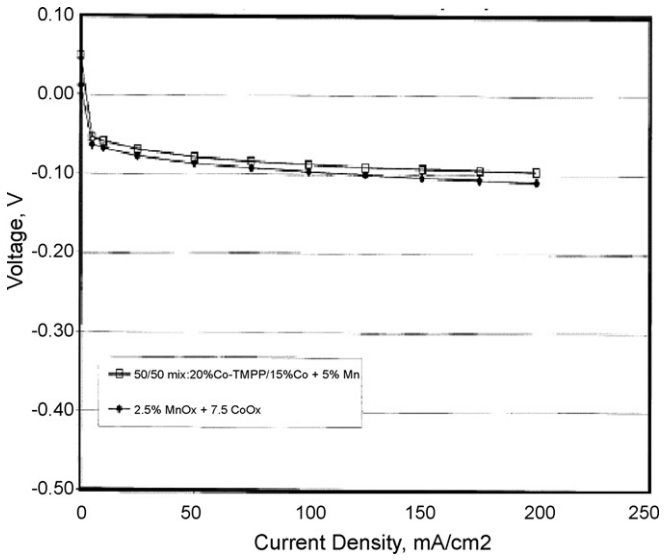

Fig. 8. ORR polarization curves for electrodes, composed of 7.5% CoO_x + 2.5% MnO_x and 50% CoTMMP + 50% (15% CoO_x + 5% MnO_x), in alkaline electrolyte [71].

1.5. Metal nitride-based ORR catalysts

Miura et al. [97] investigated the nitride-based ORR catalysts Mn_4N, CrN, Fe_2N, Co_3N, and Ni_3N in alkaline electrolyte. All catalyst had a GDL composed of 70% Acetylene carbon black AB-7 (AB-7) from Denka (specific surface area—49 $m^2\,g^{-1}$) + 30% PTFE. The cathode with a 60% Mn_4N/C + 40% Furnace Carbon Black 3000B (FCB 3000B) from Mistsubishi Kasei, catalytic coating and 15% PTFE had a maximum ORR activity of $j = 2400$ mA cm^{-2} at −125 mV (Hg/HgO) or 0.8 V (RHE) (Fig. 9). XPS analysis showed the presence of a thin oxide on the electrode surface. Mn_4N promotes the direct four-electron ORR mechanism and CO_3N decomposes HO_2^- into OH^-. This air cathode supplied stable performance during a 50 h test in galvanostatic conditions at $j = 300$ mA cm^{-2} in 9 M NaOH at 80 °C.

1.6. Mixed oxides of the transition metals

Mixed oxides on a spinel, perovskite, or pyrochlore structure are largely used for ZAFC ORR catalysts and their performances are discussed in this section.

1.6.1. Spinel-type based catalysts

1.6.1.1. $NiCo_2O_4$ (spinel). Spinels are a group of oxides with the formula AB_2O_4, where A is a divalent metal ion (such as Mg, Fe, Ni, Mn, or Zn) and B is a trivalent metal ion (such as Al, Fe, Cr, or Mn). Some of these oxides display good stability and ORR activity in alkaline solutions. Analysis of their ORR activity and stability makes it possible to select the components required for the creation of composite ORR catalysts with an optimal balance of the most important characteristics [61,97]. The stability and activity of some oxides, including La/La_2O_3, Ti_2O_3/TiO_2, Ni_2O_3/NiO_2 and Co_2O_3/CoO_2 in alkaline solution, are shown in Table 4 [98]. This stability is given by the Pourbaix diagram, which provides the equilibrium metal ion concentration for solutions of less than 10^{-6} ions/l at pH 14. The properties of the thermally prepared electrodes are given in Tables 5 and 6 [61]. NiO has a higher ORR activity than Co_3O_4, with respective current densities of 2.74×10^{-3} and 1.79×10^{-3} mA cm^{-2}. However, in contrast to Co_3O_4, NiO has four times higher H_2O_2 current efficiency and promotes the two-electron ORR pathway. Furthermore, unlike the majority of the thermally prepared oxides, Co_3O_4 is unstable during ORR (Co_2O_3 has a good stability) [98]. It was shown that spinel $NiCo_2O_4$-

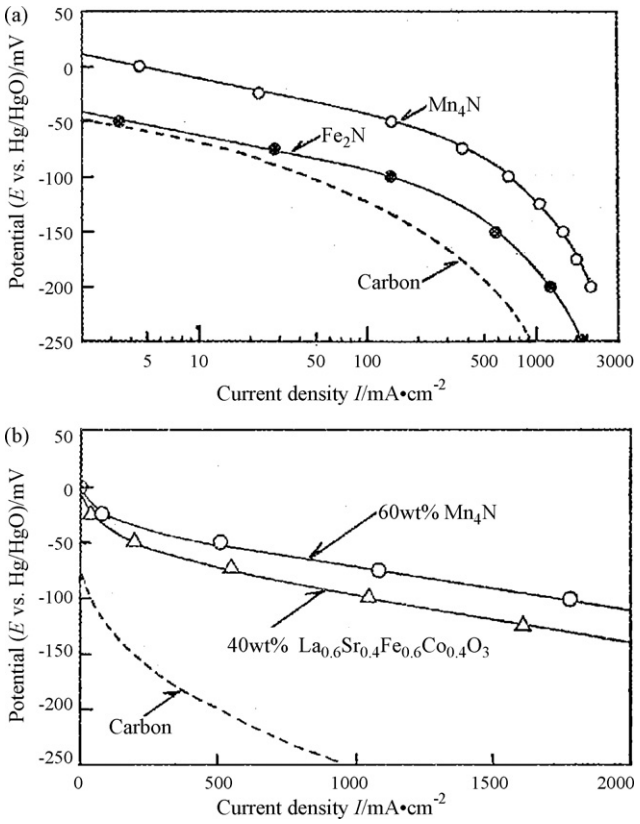

Fig. 9. ORR polarization curves for metal nitride/carbon air cathodes in 9 M NaOH and at 80 °C, with catalyst concentrations of: (a) 30% and (b) 60%. The cathodes without catalyst (carbon) and with 40% perovskite-based $La_{0.6}Sr_{0.4}Fe_{0.6}Co_{0.4}O_3$ catalyst on (b) are given for comparison [97].

based catalyst combines the desirable properties of NiO_x and CoO_x.

Cobalt has two oxides, CoO (cubic structure) and Co_3O_4 (spinel), while Ni only has NiO (cubic). CoO and NiO have similar lattice parameters, so the formation of a solid solution between them is not problematic. King and Tseung [99] discovered a correlation between the electrocatalytic activity and the structure of $NiCo_2O_4$. High, medium and low ORR activities correspond to a spinel structure, to a mixed structure of spinel and traces of cubic,

Table 4
Properties of semiconducting oxides [98].

Oxide	Electrical conductivity	Corrosion resistance at pH 14	Oxygen reduction	Potential, *V* vs. NHE
La/La_20_3	Poor	Good	Poor	−2.069
Ti_2O_3/TiO_2	Poor	Good	Poor	−0.556
V_2O_4/V_2O_3	Poor	Poor	Poor	−0.666
Cr_2O_3/CrO_2	Poor	Poor	Poor	1.284
MoO_2/MoO_3	Poor	Poor	Poor	−1.09
W_2O_3/WO_3	Poor	Poor	Poor	−0.029
Mn_2O_3/MnO_2	Fair	Doubtful	Fair	1.014
Co_2O_3/CoO_2	Poor	Good	Poor	1.44
Lower Co_2NiO_4/Co_2NiO_4	Good	Good	Good	1.4
Ni_2O_3/NiO_2	Poor	Good	Poor	1.434
RuO_2/RuO_4	Good	Poor	Good	1.387
Rh_2O_3/RhO_3	Good	Doubtful	Poor	1.73
PdO_2/PdO_3	Good	Good	Good	2.03
OsO_2/OsO_4	Good	Poor	Good	1.00
Ir_2O_3/IrO_2	Good	Poor	Good	0.93
PtO/PtO_2	Good	Good	Good	1.7
Cu_20/CuO	Poor	Doubtful	Good	0.667
AgO/Ag_2O_3	Good	Poor	Good	1.57
Au_2O_3/AuO_2	Good	Doubtful	Poor	2.63

Table 5
Tafel slopes, exchange current densities and onset potentials for ORR on the thermally prepared electrodes in 1 M KOH at $T = 25$ °C [61].

Electrode material	Tafel slope (mV dec^{-1})	I_o exchange C.D. (mA cm^{-2})	Onset potential of O_2 (mV)
NiO	−118	2.74×10^{-3}	−128
Co_3O_4 (with HCl)	−66	3.36×10^{-4}	−126
Co_3O_4 (no HCl)	−71	1.79×10^{-3}	−95
Pd*	−57	8.65×10^{-2}	−74
Pt*	−56	5.04×10^{-2}	−63
Pt	−58	8.13×10^{-3}	−78
IrO_2	−40	1.12×10^{-2}	−112
RuO_2	−225	2.17×10^{-3}	−112

Note: Pd*, Pt*—after 20 cycles of CV pre-treatment, which involved sweeping at $E = 0.4$—1.24 V (SCE) at a sweep rate of 100 mV s^{-1}.

Table 6
Current efficiencies of H_2O_2 production during ORR on thermally prepared electrodes in 1 N KOH at $T = 25$ °C [61].

Electrode material	H_2O_2 current efficiency (%)		
	0.05 mA cm^{-2}	0.1 mA cm^{-2}	0.5 mA cm^{-2}
NiO	75.4	61.7	43.2
Co_3O_4 (with HCl)	16.1	5.1	0
Co_3O_4 (no HCl)	26.9	14.7	0
Pd*	0	0	0
Pt*	4.1	0	0
Pt	21.5	5.3	0
IrO_2	55.5	40.3	10.3
RuO_2	64.6	49.8	11.1

Note: Pd*, Pt*—after 20 cycles of CV pre-treatment, which involved sweeping at $E = 0.4$—1.24 V (SCE) at a sweep rate of 100 mV s^{-1}.

and to a structure of spinel with appreciable cubic, respectively. Since Ni does not have a spinel structure, its presence in spinel $NiCo_2O_4$ is through its solubility into the Co_3O_4 matrix, with a temperature dependent solubility limited at $T > 400$ °C. $NiCo_2O_4$ is more active than CoO and NiO in 75% KOH at $T = 200$ °C, however heat treatment increases the ORR activity at temperatures below 400 °C, at which point cubic traces appear. Despite the observed structural changes, a correlation between cathode surface area and catalyst performance was not identified. The maximum corrosion current obtained in electrolyte, in the absence O_2, and at potentials ranging from $E = 1000$ to 600 mV, was 20 μA. The spinel phase is metastable, with phase transition from the spinel to cubic structure occurring at $T = 450$ °C. The performance of the ZAFC with a $NiCo_2O_4$ + PTFE air cathode is $j = 200$ mA cm^{-2} at a voltage of ~0.77 V in 5 M KOH at room temperature (Fig. 10) [99].

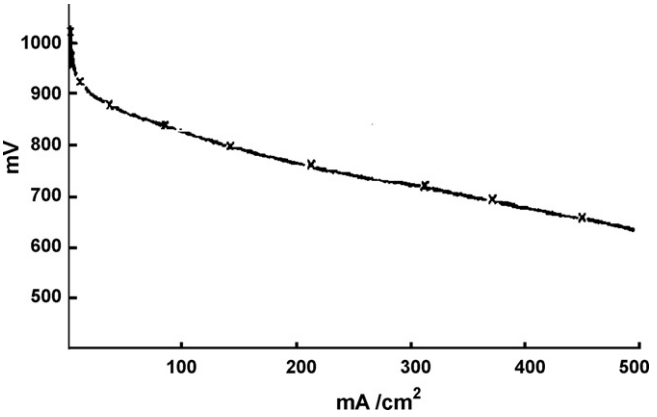

Fig. 10. The current/voltage relation for the ORR on optimized nickel–cobalt oxide [99].

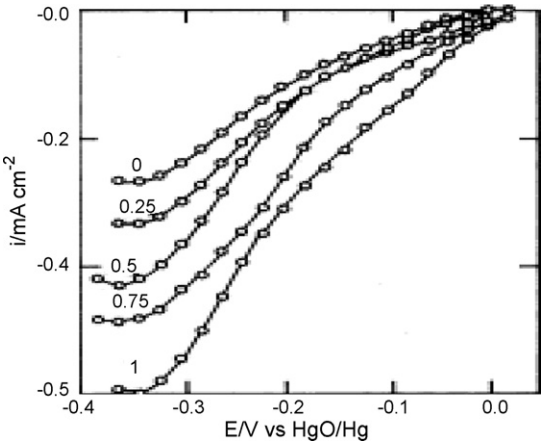

Fig. 11. Corrected current densities for the ORR polarization curves on $Mn_xCo_{3-x}O_4$ (x = 0, 0.25, 0.5, 0.75 and 1) electrodes in 1 M KOH (O_2 saturated) solution at T = 25 °C on a rotating disk electrode at 2500 rpm [100].

1.6.1.2. $Mn_xCo_{3-x}O_4$ (0 < x < 1). $Mn_xCo_{3-x}O_4$ has high electrical conductivity and ORR/OER activity. Rios et al. [100] showed that $Mn_xCo_{3-x}O_4$ has the Mn^{4+}/Mn^{3+} redox couple located in octahedral sites. Changes in the Mn^{4+}/Mn^{3+} content, as a function of x, were correlated to pH of zero charge (pH_z), rest potential ($E_{i=0}$), activation energy of conductance (E_a), and to the electrocatalytical parameters of the ORR and OER. It was observed that manganese catalyzed the ORR but inhibited the OER. The correlations between the electrocatalytic activity and the cationic distributions were investigated for the oxygen reactions in 1 M KOH at 25 °C. The corrected (real) ORR activity increases with higher Mn content. ORR polarization curves have two Tafel zones with slopes of −60 and −120 mV below and above −50 to −100 mV vs. HgO/Hg, respectively (Fig. 11). The ORR mechanism occurs via parallel paths of the four-electron and two-electron pathway. The OER activity increases with decreasing x (i.e., 1 < 0.75 < 0.5 < 0.25 < 0). Only one Tafel slope value (b_a), of ~60 mV, was measured. The OER mechanism includes fast electrosorption of OH^- and the OH radical, followed by the slow electrodesorption of OH^- into H_2O_2, which is the rate-determining step. In contrast, Co_3O_4 has an ORR active surface of Co^{3+} cations, but Mn strongly inhibits the oxidation of OH^- ions. The performance of a RDE with a $Mn_xCo_{3-x}O_4$ + PTFE coating is j = 100 mA cm^{-2} at 0.2 V.

Stability of the spinel-based catalyst in alkaline solutions was improved through electrodeposition of polypyrrole (PPy), which is electronically conductive. Gautier et al. [101] utilized a multilayered design for $Ni_{0.3}Co_{2.7}O_4$ catalysts: glassy carbon (GC) (support)/first layer of PPy/second layer of $Ni_{0.3}Co_{2.7}O_4$)/third (external layer) of PPy. The external layer of PPy protects the spinel-based catalyst against dissolution during operation in the alkaline solution. This catalyst shows an ORR activity of j = −1.4 mA cm^{-2} at −0.5 V (SCE) in an oxygen saturated 2.5 mM KOH + 0.8 M KCl solution at room temperature. The $Ni_{0.3}Co_{2.7}O_4$ has a BET surface area of 22 m^2 g^{-1}. The work [102] demonstrated that the maximum peroxide formation on $Ni_xCo_{3-x}O_4$, which takes place on the active sites such as the Co^{3+}/Co^{2+} couples, occurred at x = 0.3. The other spinel, $Cu_{1.4}Mn_{1.6}O_4$/PPy-based composition, showed good ORR activity in acidic solutions as well [102]. The spinel ($CoFe_2O_4$)/PPy with 3–30 nm particle sizes (fabricated by the microemulsion method with the use of sodium dedecyl sulphate (SDS) surfactant) showed a stable performance of j = −1.5 mA cm^{-2} at E = −0.5 V (SHE) over 8 h in an oxygen saturated 5 mM KOH + 0.5 M K_2SO_4 electrolyte at T = 25 °C. The bulk resistance was 4.5 ± 1.7 Ω for the pure polymer and 2.7 ± 0.8 Ω for the spinel/PPy composite [103].

1.6.2. Perovskite-type ORR catalysts

Perovskites are promising non-noble ORR catalysts for ZAFCs. Co and Mn-containing perovskites were investigated for oxygen reduction [99,104–111]. A detailed analysis of the stability and ORR activity for some of these catalysts in 9 M NaOH at 80 °C is given in Table 7 [111].

Table 9 shows that $LaMnO_3$ and $LaCoO_3$ have high ORR activity but insufficient chemical and electrochemical stability, as XRD analysis showed an additional phase of the lanthanum hydroxide in the composition of their structure. The additional phase indicates the instability of lanthanum. Conversely, the Fe-based perovskite, $La_{0.6}Sr_{0.4}Fe_{0.6}Mn_{0.4}O_3$, had an optimal balance of stability and ORR activity. For example, the Fe-based perovskite exhibited a performance of j = 500 mA cm^{-2} at E = −260 mV (Hg/HgO) during 70 h of testing. The ORR activity and chemical stability of 11 types of carbon, in a 9 M NaOH solution containing hydrogen peroxide, were also investigated. An evaluation was completed after 30 days and it was found that the stability and cathode performance of the investigated carbons correspondingly decreased and increased with increasing specific surface area. The EC-600JD (BET—1270 m^2 g^{-1}) and BP2000 (BET—1475 m^2 g^{-1}) have much lower chemical stability than other popular low surface area carbon blacks such as XC-72 (BET—254 m^2 g^{-1}) and AB-7 (BET—49 m^2 g^{-1}).

1.6.2.1. $LaNiO_3$. Matumoto et al. [112] established the high activity of perovskite lanthanum nickel oxide ($LaNiO_3$). It has higher ORR activity in comparison with Pt at potentials from −150 to +100 mV (vs. Hg/HgO) in 1 M NaOH. The current densities for $LaNiO_3$ and Pt at −75 mV (vs. Hg/HgO) were 2×10^{-5} and 10^{-5} A cm^{-2}, respectively.

Lamminen et al. [113] tested $LaNiO_3$ electrodes in 7 M KOH and compared their ORR activity with CoTMPP and Pt air cathodes. The electrodes were manufactured by the rolling method, the best of which were tested in long-term tests ranging from 425 to 660 h. The decay in potential during the 660 h run was 0.041 mV h^{-1}.

1.6.2.2. $LaMnO_3$. Hayashi et al. [114] used the reverse micelle (RM) and amorphous malate precursor (AMP) methods for the fabrication of $LaMnO_3$ catalysts. The electrocatalytic and corrosion

Table 7
Corrosion and electrocatalytic properties of perovskites [111].

Oxide	Chemical stability after immersion for 12 h in 9 M NaOH	Electrochemical stability at E = −260 mV (Hg/HgO)	Electrode performance (mA cm^{-2}) at E = −160 mV (Hg/HgO)
$LaMnO_3$	O	O	1266
$LaCoO_3$	X	X	1006
$LaNiO_3$	O	X	468
$LaCrO_3$	P	P	344
$LaFeO_3$	P	P	273
$La_{0.8}Sr_{0.2}FeO_3$	P	P	519
$La_{0.6}Sr_{0.4}Fe_{0.6}Co_{0.4}O_3$	P	V	682
$La_{0.6}Sr_{0.4}Fe_{0.6}Mn_{0.4}O_3$	P	P	922

Note: P—XRD detemined perovskite structure, O—perovskite + trace amounts of lanthanum hydroxide (L), V—perovskite + La, X—almost lanthanum hydroxide.

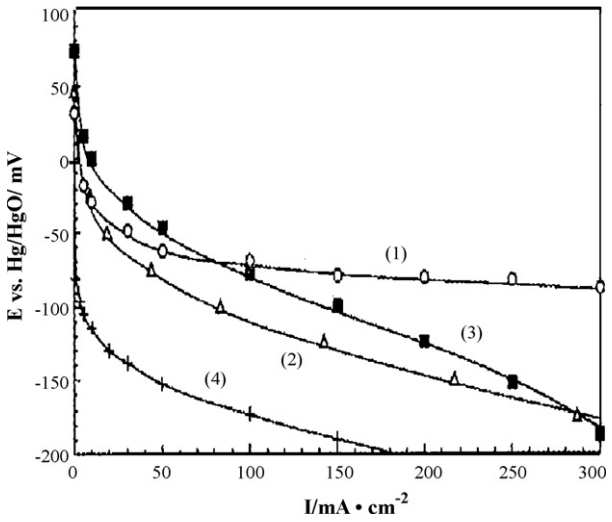

Fig. 12. ORR polarization curves for electrodes under air flow in 8 M KOH at 60 °C: (1) $LaMnO_3$ (RM method), (2) $LaMnO_{3.15}$ (AMP method) (3) Pt (0.5 mg cm^{-2}), and (4) carbon [114].

properties of these catalysts are given in Figs. 12 and 13. The stability of these electrodes was tested at galvanostatic conditions (j = 300 mA cm^{-2}). The performance of the catalyst $LaMnO_{3+\delta}$ (RM method) was maintained for 140 h (j = 300 mA cm^{-2} at − 80 mV (vs. Hg/HgO)). The higher oxidation state of $LaMnO_{3.15}$ is more active for the ORR than oxides with stoichiometric ratios.

Masayoshi et al. [115] used another modification of the reduction–oxidation precipitation in the RM method for the fabrication of $LaMnO_3$, which produced a catalyst with higher ORR activity than a catalyst produced by the hydrolysis precipitation in reverse micelle (HP-RM) method with the same particle size.

1.6.2.3. $LaCoSrO_3$. The doping of $LaCoO_3$ with Sr induces reversible behaviour in 45% KOH at room temperature with a performance of j = 2 mA cm^{-2} at 500 mV (vs. DHE) [116]. The ORR mechanism on $La_{1-x}Sr_xCoO_3$ and $Nd_{1-x}Sr_xCoO_3$ at x = 0.5 occurs via two parallel paths [117,118]:

$$(1/2)O_2 + H_2O = 2e + 2OH^- \quad (6)$$

$$O\,(\text{lattice of oxides}) + H_2O = 2OH^- + 2e \quad (7)$$

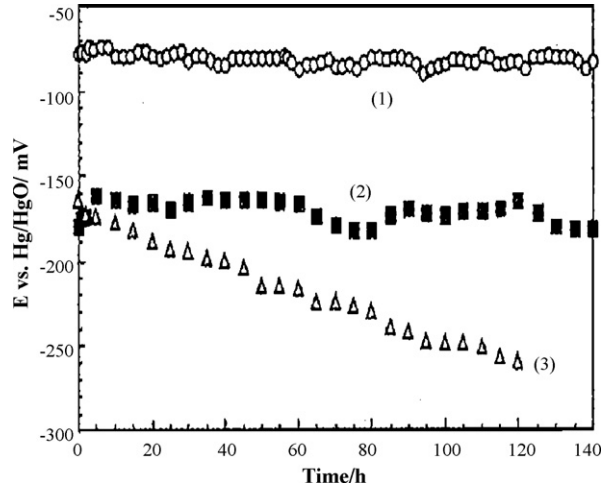

Fig. 13. Durability of the electrodes under air flow in 8 M KOH at 60 °C: (1) $LaMnO_3$ (RM method, 6.01 mg cm^{-2}), (2) $Pr_{0.6}Ca_{0.4}MnO_{3.15}$ (AMP method, 7.07 mg cm^{-2}) and (3) $La_{0.6}Ca_{0.4}CoO_3$ (7.07 mg cm^{-2}) [114].

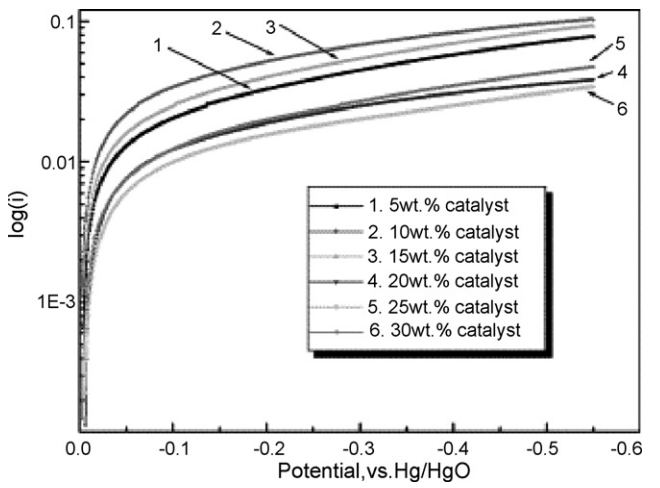

Fig. 14. ORR Tafel plots of $E - \log(j)$ for x%($La_{0.6}Ca_{0.4}CoO_3$)/C catalyst in 7 M KOH at 25 °C, where x = 5, 10, 15, 20, 25, and 30 [119].

1.6.2.4. $La_{0.6}Ca_{0.4}CoO_3$. Wang et al. [119] modified the widely studied catalyst, $La_{0.6}Ca_{0.4}CoO_3$ [120–122], by the amorphous citrate method [123]. The ($La_{0.6}Ca_{0.4}CoO_3$/C + PTFE)/C cathode has a maximum ORR activity of 20 mA at E = −200 mV (vs. Hg/HgO) in 7 M KOH at 25 °C. ORR polarization for this catalyst has two Tafel zones, which can be observed in Fig. 14.

1.6.2.5. Nd(or La)$_{0.5}Sr_{0.5}CoO_3$. The investigation of $Nd_{0.5}Sr_{0.5}CoO_3$ (BET 17 m^2 g^{-1}) and $La_{0.5}Sr_{0.5}CoO_3$ (BET 20 m^2 g^{-1}) ORR catalysts established that the rate-limiting step of ORR is dissociative oxygen chemisorption. Unlike $LaNiO_3$, the ORR activity of $Nd_{0.5}Sr_{0.5}CoO_3$ is significantly lower than Pt in 45% KOH at 25 °C [124].

1.6.3. Pyrochlore-type based ORR catalysts ($A_2B_2O_6O'$)

The cubic pyrochlore structure consists of a B_2O_6 framework with corner-shared BO_6 octahedral [125].

1.6.3.1. $Pb_2M_{2-x}Pb_xO_{7-y}$ (M = Ru or Ir). The oxide cubic pyrochlore $Pb_2Ir_2O_{7-y}$ is a good ORR catalyst in alkaline electrolyte and for the OER in acidic solution [125]. The ORR activities at 25 °C and 60 °C are similar, most likely due to decreasing electrode hydrophobicity and oxygen solubility with increasing temperature. The performance of this catalyst was $j = 6 \times 10^{-3}$ mA cm^{-2} at −100 mV (vs. Hg/HgO), while the Tafel slope of ORR polarization at $j > 6 \times 10^{-3}$ mA cm^{-2} is 60 mV decade^{-1}. Note that this catalyst does not reduce oxygen in an acidic solution. The iridium pyrochlore oxide-based catalyst has a higher stability in strong alkaline solutions in comparison with ruthenium pyrochlore oxide, while having similar ORR activity in alkaline and in partially acidic (pH > 2) solutions. Pyrochlore ($A_2B_2O_6O'$) has an active surface for OH^- species on the O′ sites (for exchange with an adsorbed $O_2^-{}_{ads}$ during ORR in alkaline solution) [125].

1.6.3.2. $Pb_2Ru_2O_{6.5}$. Lead ruthenate pyrochlore ($Pb_2Ru_2O_{6.5}$) [126] is effective in air cathodes because it promotes the four-electron ORR pathway. It can also be used as a self-supported catalyst, which avoids carbon-support oxidation. The performance of this catalyst for oxygen reduction in alkaline solution was increased by the use of a hydrogel overlayer, which was a mixture of poly(dimethyldiallyammonium) chloride and Nafion.

Finally, there are several other interesting ORR catalysts, which are not directly included in the above-mentioned group of catalysts that should be noted. These include ORR catalysts on the basis of Ni, Co, and Fe hydroxides and two Pt-based ORR catalysts [127]. Blanchart and Van Der Poorten [128] obtained a stable

voltage of 0.69 V in 6 M KOH at $T = 50\,^{\circ}C$ for catalyst 5% Pt/C. Henry et al. added Pt to Ag + MnO_2, but the performance obtained with (Ag + Pt + MnO_2 + PTFE)/C, $j = 30\,mA\,cm^{-2}$ at 1 V, was not high enough for commercial use [129].

1.7. Bifunctional air electrodes

Secondary (rechargeable) ZAFCs use bifunctional electrodes, which have active components for both the OER and the ORR. The bifunctional electrodes operate in a wide range of potentials, from 0.6 to 0.7 V (RHE) during the ORR (discharge mode) [1], to over 2.1 V (RHE) during the OER (charge mode). Additional requirements of bifunctional electrodes include higher stability of the ORR component in comparison with a primary ZAFC and a fast OER on the ORR component. Westinghouse Electric Corp. developed [130–135] promising bifunctional electrodes based on ($CuSO_4$ + $NiWO_4$ + WC + Co)/C [131,132]. The composition was subsequently modified to (3% Ag + 7% $FeWO_4$ + 7% WC + 12% Co + 7% NiS)/C. The carbon in this electrode consisted of a mixture of two different carbon blacks with high and low specific surface areas, which provided a proper balance of hydrophilic and hydrophobic properties. 22% PTFE was used as the binding agent and the silver ORR catalyst (Ag loading—2 mg cm^{-2}) was stabilized with nickel sulphide [133]. The properties of the electrode can be summarized as follows [135]:

- Silver is the ORR catalyst and it is more active than Co.
- Silver, in the presence of cobalt and nickel, improves ORR activity.
- Silver, in the presence of sulphides (NiS), forms Ag_2S, which is relatively stable in alkali electrolyte.
- Hydrated cobalt oxide promotes decomposition of the hydroxides produced during the ORR.
- WC and Ni–Fe hydrated oxides (the latter forms during charging) are ORR catalysts with high activity.

Another of Westinghause's improved bifunctional electrodes was developed by Liu and Jackovitz [136] and consisted of ($AgCoWO_4$ + WC + WS_2 + NiS + 10–15% Co)/C + 20% PTFE. The electrode composition does not allow gas pockets to form between the air cathode and electrolyte, due to gas evolution, during discharge. It is by this mechanism that the chemical reaction between electrolyte and air cathode is interrupted and decreases cell performance.

Shepard et al. [137] developed other bifunctional electrodes with complex ORR catalyst compositions similar to the OER catalyst from Westinghouse: ORR catalyst [(0.3–2%) CoTMMP/C + (1–4%) Ag + (1–7%) NiS(or WS_2) + (4–10%) $LaNi_{1-x}Co_x$ + (18–32%) Co_xO_y] + OER catalyst [(1–20%) WC + (1–20%) Co + (1–7%) $FeWO_4$ (or $CoWO_4$)/C (AB-50)]. The fabrication method of this electrode included the following procedures:

- The Co + WC mixture was sintered.
- AB-50 was treated with CoTMPP and Ag.
- The Ag/C was prepared by mixing a carbon black and silver nitrite solution followed by reduction with hydrazine.
- The CoTMPP solution was added to the silverized carbon black (Ag/C) and subsequently sintered at 750 °C for 1 h in inert gas.
- KOH was added as a wetting agent and ammonium carbonate was added for pore formation.
- Different concentrations of the ORR and OER catalysts were used in various layers for protection against the formation of gas pockets between the air electrode and electrolyte (2% more OER catalyst was used on the airside and 0.6% more ORR catalyst was used on the electrolyte side).

Table 8
Composition of the catalyst and gas diffusion layers of the multilayer bifunctional electrode [137].

First sublayer of active layer (electrolyte side):
19.5%(AB50 + 2% CoTMPP + 8% Ag) + 23.6% Co_xO_y + 4.8% $LaNi_{0.9}Co_{0.1}O_y$ + 1.4%(WC + 12% Co) + 1.4% $FeWO_4$ + 1.4% NiS + 8.4% KOH + 14.2% NH_4HCO_3 + 2.8% carbon fibers + 22.3% Teflon
Second sublayer of active layer (air side):
20.7%(AB50 + 2% CoTMPP + 8% Ag) + 22.6% Co_xO_y + 4.6% $LaNi_{.9}Co_{.1}O_y$ + 3.1%(WC + 12% Co) + 3.1% $FeWO_4$ + 3.1% NiS + 7.5% KOH + 13.6% NH_4HCO_3 + 2.7% carbon fibers + 19% Teflon
Wet-proofing layer:
50.4% untreated AB-50 + 7.2% carbon fibers + 42.5% Teflon

Table 9
Air—cathode design [138].

1. GDL—a porous layer, composed of 65% carbon (ammonium bicarbonate) + 35% PTFE, that allows gas penetration while preventing liquid penetration
2. AL—active layer, composed of hydrophobic and hydrophilic pores (the latter for ORR) containing 10–30% catalyst ($MnSO_4$ + La_2O_3 or MnO_2 + La_2O_3) + 50–60% High SA carbon black + 15% PTFE
3. OEL—oxygen evolution layer, requires hydrophilic pores for electrolyte penetration and the OER and contains 45% OER catalyst + 50% High SA carbon black + 5% PTFE. Ammonium bicarbonate was also utilized for pore formation

- The three layer electrodes were dried at 85 °C for 120 min and hot-pressed at $T = 300\,^{\circ}C$ and $p = 0.5$ ton $in.^{-2}$ for 10 min.

The electrode design, detailed in Table 8, consists of an active layer (AL) with two sublayers (0.02 and 0.025 in thick) and a 0.015 in thick wet-proofed GDL layer.

The OEL has high surface area carbon black and pore-former to control electrolyte flooding. Two of the examined catalyst compositions for this electrode were 63.5% Vulcan XC500 (XC-500) from Cabot + 13% $MnSO_4$ + 8.5% La_2O_3 + 15% PTFE and 69% XC-500 + 8% MnO_2 + 8% La_2O_3 + 15% PTFE [138]. If the AL and OEL are combined into a single layer, then the optimal ratio of OER catalyst/ORR catalyst is 40:60 in the bifunctional catalyst (Table 9). Fig. 15 shows that the ORR activity of the combined catalyst ($MnSO_4$ + La_2O_3, BET—12.5 $m^2\,g^{-1}$) in alkaline electrolyte exceeds the activity of the same catalysts separately. The test was carried out in a half-cell with a Ni counter electrode. Although the stability of La_2O_3 was better than that of $MnSO_4$, it was found that the stability of the combined catalyst was higher [138].

The replacement of $MnSO_4$ with the same concentration of MnO_2 led to a decrease in the discharge voltage (vs. Zn at

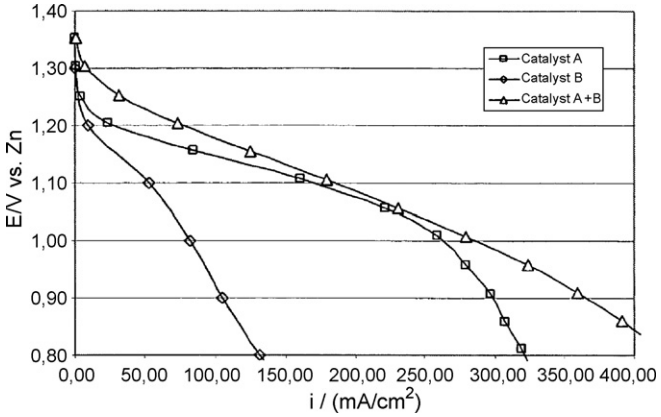

Fig. 15. ORR polarization curves for air electrodes in 6.6 M KOH—(A) $MnSO_4$, (B) La_2O_3, and (A + B) La_2O_3 + $MnSO_4$ [138].

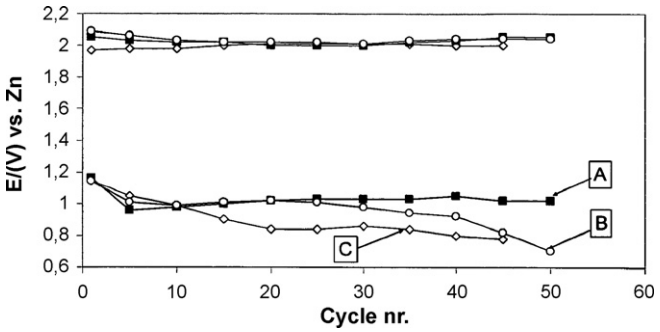

Fig. 16. Stability of air electrodes in 6.6 M KOH at a charge/discharge rate of 100 mA cm^{-2} and a discharge capacity of 626 mAh cm^{-2} per cycle. (A) 19% Ag + 8% $MnSO_4$, (B) 19% Ag, (C) 19% Ag + 8% La_2O_3 [138].

100 mA cm^{-2}) from 0.98 to 0.88 V. Increasing the percentage of ORR catalyst led to an increase in the discharge voltage and a decrease in the stability during a cycling test, whereas, an increase in the percentage of OER catalyst led to the opposite situation. The best ratio of OER catalyst to ORR catalyst was 5–20%:5–15%. The replacement of the OER/ORR active La_2O_3 with Ag led to an increase in charge/discharge stability. Fig. 16 shows the charge and discharge potentials over the course of 50 cycles for the pure Ag electrode (B) and Ag combined with $MnSO_4$ (A) and La_2O_3 (C). As shown in Fig. 16, 19% Ag + 8% $MnSO_4$ showed higher stability and discharge voltage than pure Ag, while 19% Ag + 8% La_2O_3 has sufficient stability but a low discharge voltage.

Coetzer et al. [139] investigated the use of different carbides for bifunctional electrodes in the alkaline electrolyte of Li-ion batteries. Several carbides, including TaC, WC, W_2C, TiC, Cr_3C_2, Cr_7C_3, $Cr_{23}C_6$, MoNiC, and WCoC, were tested for the evaluation of their stability and ORR activity in alkaline electrolyte. TiC and VC showed the worst ORR activity, MnC_3 also demonstrated low ORR activity at low temperatures, and both Cr_2O_3 and FeC were unstable in alkaline electrolyte and had low ORR activity. The best ORR activity was obtained with a composition of TaC + WC + W_2C + TiC.

Zhimin [140] developed a three-electrode secondary ZAFC, consisting of an ORR cathode with CoTMPP and an OER electrode composed of 30% Ag + 70% $LaNiO_3$. The addition of Ag to $LaNiO_3$ decreased the formation of ZnO, by decreasing the affinity of $LaNiO_3$ for ZnO.

1.7.1. $La_{1-x}A_xFe_{1-y}Mn_yO_3$ (A = Sr or Ca)

Perovskites are the group of oxides with formula ABO_3, where A is a divalent metal ion (i.e., Ce, Ca, Sr, Ca, Pb, and rare earth metals) and B is a tetrahedral metal (i.e., Ti, Nb, Fe). Shimizu et al. [141] suggested promising bifunctional perovskite-based catalysts, with high ORR and OER activity, on the basis of $La_{1-x}A_xCoO_3$ (A = Sr or Ca) [141,142] and $La_{0.8}Sr_{0.2}BO_3$ (B = Co, Mn, or Fe) [143,144]. In these works, it was discovered that the comparative activity of $La_{0.8}Sr_{0.2}BO_3$ (B = Co, Mn, or Fe) catalysts for ORR and OER decreased Co > Mn > Fe and Co > Fe > > Mn, respectively. Unfortunately, even though the Co-based catalysts were shown to have the highest OER and ORR activity, they did not have sufficient stability in the alkaline electrolyte [143]. This was one of the main reasons for the development of the Co-free catalyst with the composition of $La_{1-x}A_xFe_{1-y}Mn_yO_3$ [143]. The type and concentration of Sr or Ca at the position A-site in the perovskite structure strongly affects the ORR activity. For example, $La_{0.8}Sr_{0.2}Fe_{1-y}Mn_yO_3$-catalyst has maximum ORR activity at $y = 0.6$ and maximum OER activity at $y = 0.2$. The $La_{1-x}Ca_xFe_{0.8}Mn_{0.2}O_3$ catalyst demonstrates maximum ORR (200–300 mA cm^{-2} at −300 mV (Hg/HgO) in 7 M KOH at 25 °C with air flow) and OER activities and maximum BET surface area at $x = 0.4$ [143].

OER activity depends on the type of cation on the A-site and is ranked accordingly: Sr > Ca > Ba > La. Increasing Mn concentration to 60% leads to an increase ORR activity, but the maximum OER activity is at $y = 0.2$. The ORR reduction on Co-based perovskite catalysts in 7 M KOH proceeds via the two-electron pathway and it is rate-determined by the HO_2^- decomposition reaction: $O_2 + H_2O + 2e = HO_2^- + OH^-$. The rate of HO_2^- decomposition and OER and ORR activity (normalized per unit surface area) increase for the Co-free perovskite catalyst, $La_{1-x}Ca_xFe_{0.8}Mn_{0.2}O_3$. Thus, the HO_2^- decomposition reaction is rate-determining for both processes, the ORR and OER. Note that Sr increases the surface areas of the mixed perovskite-based catalysts [145].

1.7.2. $La_{0.6}Ca_{0.4}Co_{0.8}B_{0.2}O_3$ (B = Mn, Fe, Co, Ni, or Cu)

Shimizu et al. [145] developed $La_{0.6}Ca_{0.4}Co_{0.8}B_{0.2}O_3$/C (B = Mn, Fe, Co, Ni, or Cu) with a maximum bifunctional activity for B = Fe (1 M NaOH at 25 °C, $j = 200$ mA cm^{-2} for the ORR and 300 mA cm^{-2} for the OER at −150 and +620 V (Hg/HgO) respectively). The Fe-based catalyst also demonstrated a high activity for the decomposition of the HO_2^- intermediate. These electrodes were synthesized by the amorphous citrate precursor (ACP) method. The effect of the B-site metal on the BET surface area and the HO_2^- decomposition activity in 1 M NaOH at 25 °C was determined based on the rates of oxygen evolution from the decomposition of H_2O_2 in 7 M NaOH at 80 °C [143]. The decomposition activity, K_w (the amount of O from H_2O_2 per g of oxides), is given in Fig. 17. The majority of oxygen reduced on the developed electrode proceeds via the two-electron mechanism, but only under working current densities is the ORR rate is determined by the HO_2^- decomposition rate. The four-electron mechanism of ORR was only observed at low current densities. The electrode with B = Fe produces the maximum BET surface area of 28 m^2 g^{-1} and rate of HO_2^- decomposition, while electrodes with B = Mn, Co, Ni, and Cu had BET surface areas of 18, 18, 17, and 4 m^2 g^{-1}, respectively.

1.7.3. $La_{0.6}Ca_{0.4}CoO_{3-\delta}$ and $La_{0.7}Ca_{0.3}CoO_{3-\delta}$

Lippert et al. [146] tested $La_{0.6}Ca_{0.4}CoO_{3-\delta}$ and $La_{0.7}Ca_{0.3}CoO_{3-\delta}$ as bifunctional air catalysts for ZAFC. These catalysts, which have an amorphous structure, mixed orientation or single orientation, were produced by pulsed laser deposition. Catalysts with mixed or single orientations showed higher OER/ORR activity in a ZAFC in comparison to those with an amorphous structure.

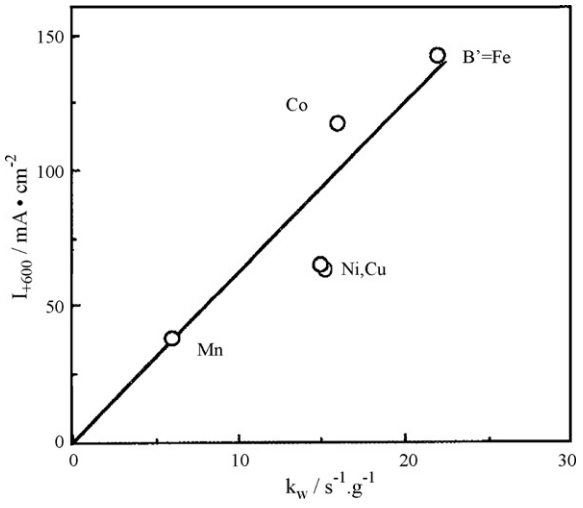

Fig. 17. The anodic current densities of $La_{0.6}Ca_{0.4}Co_{0.8}B_{0.2}O_3$ (B = Mn, Fe, Co, Ni, or Cu), corrected with the catalytic activities for the decomposition of HO_2^- (K_w) [143].

Table 10
Summary of porosimetry measurement for commercial carbon blacks [72].

	Shawinigan Black AB-50	Vulcan XC-72R	Black Pearls 3700
Total cum, volume ($mm^3\ g^{-1}$)	378.5	362.5	248.5
Spesific surface area ($m^2\ g^{-1}$)	13.9	18.1	7.5
Pore radius average (μm)	0.063	0.030	0.086
Bulk density ($g\ cm^{-3}$)	2.4	2.5	3.2
Total sample porosity (%)	47.3	47.5	44.5
KOH adsorption volume ($mm^3\ g^{-1}$)	63.1	75.4	147.6
Wet pore/total cum, volume	0.17	0.21	0.59

2. Design of ZAFC air cathodes

Analysis of the patent literature showed that a typical air cathode design for a primary ZAFC consists of:

- Teflon membrane on the air side with a high air permeability of 2000–4000 s (Gurley method). The main producer for battery applications is W.L. Gore and Associates (USA). This membrane protects the air cathode against possible leakage of electrolyte to the current collector.
- Current collector, typically a Ni mesh, a cheaper woven copper mesh with Ni coating (mesh size 0.6 mm × 0.6 mm), or an expensive Ni foam. Some of the main producers of Ni mesh are Unique Wire Weaving Co. (USA) and Dexmet Corp. (USA). Ni foam is produced by Inco (USA). Ni foam has a higher surface area and increases the performance of the air cathode.
- Gas diffusion layer, AB-7 with low BET surface area and wettability + PTFE or FEP. The use of acetylene blacks with higher hydrophobic properties promotes more hydrophobic GDL properties.
- Catalyst layer: catalyst + carbon black with high BET surface area + PTFE.
- Optional second current collector (included into the catalyst layer on the electrolyte side) for additional mechanical strength from nickel mesh, a metal mesh with a nickel coating or another metal coating, which is the same as the ORR catalyst. The main producers of air cathodes are: eVionyx Inc. (USA), Powerzinc Electric Inc. (China), Fuel Cell Technologies Inc., Gaskatel GmbH (Germany), and Yardney Technical.
- Secondary ZAFC development significantly improved the above-mentioned primary ZAFC air cathode design by:
  (a) Combining carbon blacks [38–40,130,133,137] with high and low surface areas provides better control of the electrolyte permeability of the hydrophilic catalytic layer, due to the change in permeability with changing concentration of high surface area carbon (higher concentrations improve the hydrophilic properties). It was found that the use of low surface area carbon black improved the OER. The electrolyte wetting of the hydrophobic layer is determined by the extent of the fissures within the GDL and the high surface area carbon content. An example from the literature [38] includes: catalyst layer—5% MnO_2 (Mn^{3+}/Mn^{4+}) + 70% C (60% PWA activated carbon (PWA) from Calgon + 40% EC-600JD + PTFE; and GDL—30% EC-600JD + 70% AB-50 + PTFE.
    – low SA carbon blacks are AB-50 and AB-7.
    – high SA furnace carbon blacks are AB-50 EC-600JD or FCB 3000B.
  (b) Combining different hydrophobic agents with dissimilar melting temperatures, such as PTFE and FEP (T_{melt} = 270 °C) [129,131]. The use of FEP as the binding agent instead of PTFE allows for a reduction in the heat treatment temperature, which decreases carbon oxidation.
  (c) Utilizing different Teflon concentrations in the GDL and catalyst layer [64,132]. The optimal balance of the hydrophilic and hydrophobic properties of air cathodes is achieved with PTFE concentrations of 30–70% in the GDL and 10–30% in the active layer.
  (d) Utilizing different catalyst concentrations on the air and electrolyte sides of the electrode [137]. Gas pocket formation between the electrolyte side of air cathodes and migration of electrolyte into the catalyst layer pores can be prevented through the use of different OER and ORR catalyst concentrations in the active layer coating [134]:
    – The ORR catalyst concentration is 0.5% higher on the electrolyte side of the AL than on the air side.
    – The OER catalyst concentration is 5% lower on the electrolyte side of the AL than on the air side.

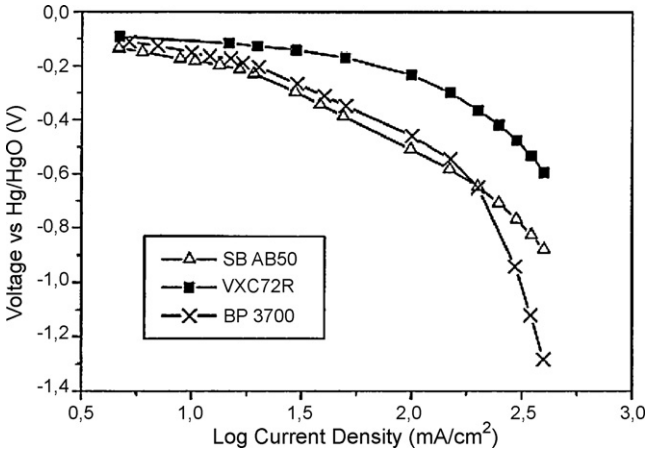

Fig. 18. ORR polarization curves for uncatalyzed carbon blacks, AB50, XC72, BP3700 in 7.5 M KOH, T = 25 °C under air flow and after polarization at j = 200 mA cm^{-2} for 1 h [72].

The properties of the carbon are key factors in producing high performance ZAFC air cathodes. For example, carbon corrosion in the catalyst layer increases by 10% when high surface area carbon is used [137]. Some of these properties are given in Tables 10 and 11 and Figs. 18 and 19 [149].

Excessive electrode wetting is a common cause of low cathode performance. High wettability of a catalyst surface prevents the diffusion of oxygen to the catalyst layer reactive sites and reduces the effective area of the three-phase (gas–solid–liquid) interface, thereby leading to poor performance. Therefore, the GDL should contain hydrophobic carbon blacks, such as acetylene carbon blacks [107], but active layers should balance the hydrophobic and hydrophilic properties for the gas–solid–liquid interface. This balance can be achieved with a mixture of hydrophobic acety-

Table 11
Comparison of radius (r) and length (l) of pores and active specific surface (S) of porous mass, as obtained from porosimetry (por), permeation (perm) and impedance spectroscopy (imp) measurements [72].

Carbon	R_{1px} (μm)	R_{2px} (μm)	R_{perm} (μm)	R_{imp} (μm)	S_{por} ($m^2\ cm^{-2}$)	S_{imp} ($m^2\ cm^{-2}$)	l (cm)
Shawinigan Black AB-50	0.038	0.20	0.25	0.40	12.61	10	0.015
Vulcan XC-72R	0.024	0.26	0.25	0.30	22.70	15	0.020

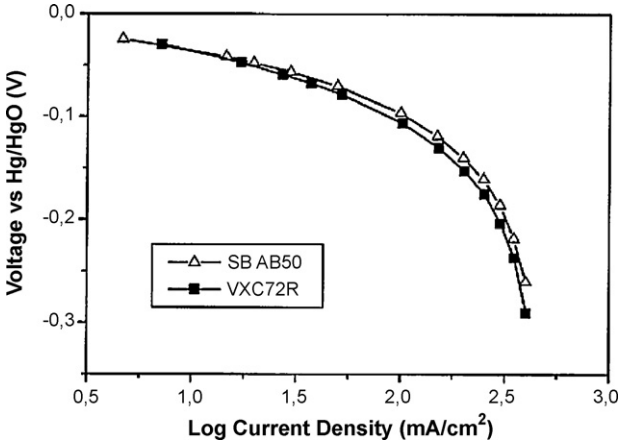

Fig. 19. ORR polarization curves for 10% CoTMPP/C catalyst utilizing either XC72 or AB50 in 7.5 M KOH, $T = 25\,^{\circ}C$, under air flow and after polarization at $j = 200\,mA\,cm^{-2}$ for 1 h [72].

lene carbon blacks (ACB) and hydrophilic furnace carbon blacks (FCB). AIR Energy Resources, Inc. (USA) used a 70:30 ratio between ACB (AB-50) and FCB (EC-600JD) for optimal electrolyte and oxygen permeability in the catalyst layer and the formation of the gas–solid–liquid interface of their MnO_2-based catalyst [37].

A higher concentration of ACB in the catalyst is also desirable for reasons of stability and activity since ACB demonstrates high activity, despite a low surface area due to a bimodal pore structure. The AB-50 has two types of pores: the first group has an average diameter of 30 nm [72] and the second group pores has a 200 nm diameter with 40 nm carbon particles. The higher BET surface area of FCB promotes high ORR activity but, unfortunately, promotes catalyst dissolution as well.

Eom et al. [147] established that the ratio of the specific surface area between the meso/macropores (A) and micropores (B) in the carbon more strongly effected the performance of ZAFCs than their total BET surface area. The activated carbon, Darco G-60N, with a ratio of A:B = 1:1 and BET specific surface area (SSA) 853 $m^2\,g^{-1}$, has a positive effect on performance in comparison with carbon BP20, with a ratio of A:B = 1:30 and BET SSA 1929 $m^2\,g^{-1}$, due to a higher number of air flow channels and reaction sites. Muller et al. [148] observed a decrease in the activity and an increase in durability and crystallinity of the graphitized carbon black Vulcan XC-72R at 2700 °C (BET SSA 70 $m^2\,g^{-1}$). They also observed that Ketjen carbon black, with surface area 1200 $m^2\,g^{-1}$, has low durability in a ZAFC. Zhang et al. [149] discovered an increase in ZAFC performance through the use of mesocarbon microbeads (MCMB) in an air cathode composed of MnO_2/MCMB.

Addition of a semiconducting layer (with a p–n-type junction) between the air side and the electrolyte side of the active layer has been shown to improve the performance of bifunctional electrodes [150]. The main problem for bifunctional electrodes is unwanted gas evolution during charge and discharge, which increases the pressure on the gas-side of the electrode. This pressure increase leads to corrosion, deactivation of the catalyst and a shortened lifetime. The p–n junction diode forms a Shottky barrier junction, which essentially causes the air side of the electrode to become electrically inactive during the charge cycle. During discharge, however, electrons can flow freely into the air side for the ORR. This rectifying layer is based on Te, SbBi, Sb, Si, GeTe, InAs, InSb, $CdSnAs_2$, or GaSb.

Table 12
ORR catalyst preparation methods.

Method	Catalyst	Reference
1. Sol–gel with reduction	MnO_2	[37,39]
2. Reverse micelle	MnO_2, $LaNiO_3$	[38] for MnO_2 [111] for $LaMnO_3$
3. Reduction of inorganic metal salts, followed by heat treatment	MnO_2	[31]
4. Co-precipitation	MnO_2, $LaNiO_3$	[97,140] for $LaNiO_3$
5. Pyrolysis	Co/FeTMPP, $NiCo_2O_4$, $Mn_xCo_{3-x}O_4$	[99] for $NiCo_2O_4$ [100] for $Mn_xCo_{3-x}O_4$

3. Fabrication methods for ORR catalysts

The main methods of ORR catalyst fabrication for ZAFCs are summarized in Table 12.

An analysis of catalyst preparation methods (Table 12) shows that the most popular methods are the sol–gel and co-precipitation methods. The best stability and ORR activity for CoTMPP and FeTMPP are achieved with heat treatment at 800 °C in inert gas for 5–6 h.

The patent literature shows an opportunity for increasing performance of ORR catalysts by using dispersants (non-ionic surfactants) to increase the surface tension between the PTFE particles and the other components of the active layer [137,140] and the adhesion of the metals to the carbon support. For example, Daxad increases silver adsorption on carbon black [48].

Examples of two fabrication methods for perovskites, co-precipitation and reverse micelle, are given below [140]:

3.1. Co-precipitation method

The co-precipitation method consists of mixing Ni and La nitrate solutions, followed by precipitation of their hydroxide at high pH. After washing, drying and heat treatment at $T = 700$–$800\,^{\circ}C$, the final perovskite product is obtained. The procedures of $LaNiO_3$ synthesis are shown below:

1. Dissolve the $Ni(NO_3)_3$ and $La(NO_3)_3$ in H_2O.
2. Adjust the pH of the solution, through the addition of 1 M NaOH, to form La and Ni hydroxides.
3. Centrifuge and wash the deposits of La and Ni hydroxides to remove the sodium ions and soluble salts.
4. Dry the deposits at 100 °C.
5. Heat at 800 °C in O_2 for 16 h to form $LaNiO_3$.

3.2. Reverse micelle method

Subject a mixture of two solutions, A (La–Mn nitrates) and B ($N(CH_3)_4OH$), to aging, centrifuging, separation, washing with ethanol and water, drying at 120 °C, and sintering at 600 °C. The carbon powder was added to solution A and heat treatment was performed in a nitrogen atmosphere to prevent carbon combustion. The procedure for carbon addition is very important, as it was discovered that a cathode fabricated from ink containing carbon that was added to solution A had higher ORR activity than one fabricated from an ink containing carbon that was added to the oxides, due to poor oxide dispersion. AMP, the typical method of fabrication for perovskite mixed oxides experiences heavy coagulation with carbon black. The RM directly synthesizes the oxides on the carbon particles and particle-formation occurs within the nano-sized reverse micelles. An example of the RM method for $LaMnO_3$ fabrication is given in Fig. 20 [114].

As can be seen in Table 13, the method of fabrication can have a large effect on the durability of the resulting catalyst. The durabil-

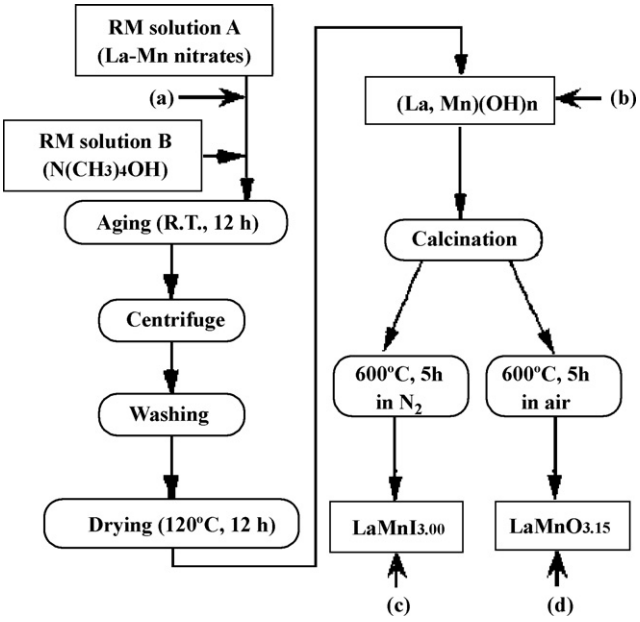

Fig. 20. The scheme of the reverse micelle method for $LaMnO_3$ fabrication and the stages, (a) through (d) (indicated by arrows), at which the carbon powder was introduced to the oxide or its precursor [114].

ity was estimated according to the absolute value of the potential change (galvanostatic polarization) at $j = 300\ mA\ cm^{-2}$.

4. Discussion

4.1. MnO_x

The most common ORR catalyst for primary ZAFCs (MnO_2) does not have sufficient ORR activity, but it is sufficiently active for hydrogen peroxide decomposition and stable in alkaline solution. MnO_2 promotes the two-electron pathway of the ORR and MnOOH has higher ORR activity than oxides such as Mn_2O_3, Mn_3O_4, and Mn_5O_8 due to an increase in the number of active centers. Doping of Mn_xO with Mg and Ni led to significantly improved ORR activity and selectivity towards the four-electron pathway of ORR.

4.2. Ag

Ag has good stability and high ORR activity in alkaline electrolyte. Ag on CNC ($333\ m^2\ g^{-1}$, 15–30 nm) demonstrated better performance ($E = 0.99$ V at $200\ mA\ cm^{-2}$) in comparison with commercially available Mn and MnCo-catalyzed air cathodes. Another promising Ag-based catalyst is Ag:W_2C = 1:1/C, with an ORR activity surpassing that of Pt/C. While Ag is a precious metal, it is one of the cheapest. Its price on the London Metal Exchange is $17.125 per troy oz, which is about 110 times less than the platinum price of $1963 oz^{-1} (July, 2008) [151]. Regardless, its concentration is very limited (5–15%) in the more efficiently developed air cathodes. The most effective Ag-based air cathode catalysts consist of Ag/C, $AgMnO_4 + MnO_2$, AgO-$LaNiO_3$, and (Ag + WC = 1:1)/C.

4.3. $CoO_x + MnO_x$/C-based catalyst

The combination of CoO_x (which is ORR active but unstable in alkaline electrolyte) with MnO_2 (which is stable and active for H_2O_2 decomposition) into 2.5% MnO_x + 7.5% CoO_x/C results in a high ORR activity of $120\ mA\ cm^{-2}$ at −0.1 V.

4.4. Co/FeTMPP

CoTMPP has higher electrochemical stability than FeTMPP, but has lower ORR activity. Unlike CoTMPP, which promotes the two-electron ORR pathway, FeTMPP promotes direct four-electron reduction. The stability of the following metal macrocyclic complexes, which depends on the metal, are ranked as following: Co > Fe > Mn. The presence of carbon during the pyrolysis of CoTMPP plays a key role in the ORR activity of CoTMPP/C, but not its structure. 10% CoTMPP/C (C—activated carbon), with 5 h of heat treatment in Ar at $T = 460$–$850\ ^\circ C$, demonstrated a performance of $200\ mA\ cm^{-2}$ at −200 mV (Hg/HgO), in 7 M KOH at room temperature. Doping CoTPMM with MnO_2 gives one of the highest ORR performances for a primary ZAFC: $j = 216\ mA\ cm^{-2}$ at 1 V, in 30% KOH at $T = 25\ ^\circ C$.

4.5. Manganese nitride

Mn_4N is one of the ORR active catalysts that promote the direct four-electron pathway. It has a stable performance at −125 mV (Hg/HgO) in 9 M NaOH at 80 °C:

- For 5 h at $j = 2400\ mA\ cm^{-2}$.
- For 50 h at $j = 300\ mA\ cm^{-2}$.

4.6. Spinel $NiCo_2O_4$

Spinel $NiCo_2O_4$ is one of the few non-noble compounds, which simultaneously have high stability and ORR activity in alkaline electrolyte. It is more active than CoO and NiO in 75% KOH at $T = 200\ ^\circ C$. The performance of a ZAFC with a $NiCo_2O_4$ + PTFE air cathode in 5 M KOH is $j = 200\ mA\ cm^{-2}$ at 0.87 V and room temperature.

4.7. Perovskite $La_{0.6}Sr_{0.4}Fe_{0.6}Mn_{0.4}O_3$

The perovskite-based ORR catalysts $LaMnO_3$ and $LaCoO_3$ have high ORR activity, but insufficient stability. However, $LaMnO_3$ after doping with Sr and Fe ($La_{0.6}Sr_{0.4}Fe_{0.6}Mn_{0.4}O_3$) demonstrates significantly improved stability as a ZAFC cathode: $j = 500\ mA\ cm^{-2}$ at −260 mV (Hg/HgO) for 70 h. The other promising perovskite compositions ($La_{0.6}Ca_{0.4}Co_{0.8}B_{0.2}O_3$ (B = Mn, Fe, Co, Ni, Cu)) promote the two-electron ORR pathway at high currents and the four-electron pathway at low currents. Among perovskites, $La_{0.6}Ca_{0.4}Co_{0.8}Fe_{0.2}O_3$ has one of the highest BET surface areas ($28\ m^2\ g^{-1}$) and HO_2^- decomposition rates.

Table 13
Fabrication method and durability of ORR catalysts [114].

ORR catalyst	Method	Potential (mV vs. Hg/HgO) at 300 mA cm^{-2} in 8 M KOH and 60 °C after τ (h)	
		$\tau = 0$	$\tau = 120$
$LaMnO_3$	Reverse micelle method (loading of 6 mg oxides cm^{-2})	80	80
$Pr_{0.6}Ca_{0.4}MnO_3$	AMP method	170	160
$La_{0.6}Ca_{0.4}CoO_3$	AMP method	165	240

Table 14
ZAFC air cathodes.

Assignee	Catalyst composition	Air cathode design	Performance	Catalyst fabrication method	Reference
MnO_2-based ORR catalyst					
Rayovac Corp. (USA)	MnO_2 + C + PTFE	Standard[a]		$KMnO_4$ reduction	[31]
R.B. Dopp et al.	Mn isopropoxide + activated C + 12% PTFE	Standard[a]			[36]
AER Energy Resources Inc. (USA)	5% MnO_2 + 75% C (mixture of 30% EC-600JD and 70% AB-50) + 20% PTFE	Standard[a]	No data	Sol–gel	[37]
AER Energy Resources Inc. (USA)	5% MnO_2 (Mn^{3+}/Mn^{4+}) + 70% C (60% PWA + 40% carbon black) (PTFE-Teflon 30B) GDL: 30% EC-600JD + 70% AB-50	Standard[a]	No data	Micelle encapsulation with two non-ionic surfactants	[38]
Rayovac Corp. (USA)	MnO_2 + C (activated carbon + BP2000) + PTFE. Particle size distribution MnO_2—20–26 μm	Standard[a]	Voltage of 1.15 V at 150 mA cm^{-2} is more stable over 15 h than the prior art in 30% KOH	Sol–gel (reduction of $KMnO_4$ by sodium formate at pH 7)	[39]
Matsushita Electrical Industrial Co., Ltd.	30% MnO_2 + 20% active carbon + 20% carbon black + 30% PTFE	Standard[a]	No data	Heat treatment of the gamma manganese oxyhydroxide at 250–450 °C with product: Mn_5O_8 + beta MnO_2 in air 250–300 °C	[40]
Gore Enterprise Holdings, Inc. (Newark, DE)	20% MnO_2 + 66% C + 14% PTFE	Standard[a]	Limiting current of 11 mA cm^{-2} (commercial 50–100 mA cm^{-2})		[41]
F. Sun et al.	Catalyst layer: 20% MnO_2 + 70% active carbon + 10% PTFE GDL: 15% carbon black + 85% PTFE	Standard[a]	Discharging voltage cell 1.32 V after 1 h at impedance for a 620 Ω load and 1000 Hz		[42]
Duracell Inc. (USA)	11% gamma MnO_2 + 41% C (BP2000) + 48% PTFE		ZAFC output of 430 mAh to 1 V cutoff is 7.5% better than prior art. Deliver the first 400 mAh of capacity at 300–400 mV higher than prior art.	Milling of MnO_2 and a carbon black	[43]
Duracell Inc. (USA)	MnO_2 cathode + PTFE + 2–20% absorbent material such as the gelling material used in the anode.	Standard[a]	Limiting current of 27.5 mA at 66 °C		[44]
Duracell Inc. (USA)	MnO_2	Standard[a]	Energy density of ZAFC 0.1–0.3 Wh g^{-1} MnO_2 at a 1 A discharge to 0.8 V cutoff voltage.		[47]
F. Sun et al.	MnO_2	Standard[a]	Discharging voltage after 1 h at 620 and 150 Ω 1000 Hz AC for the stack with 10 cells: 3-layer cathode: 1.31, 1.25, 4.0 V 2-layer cathode: 1.3, 1.18, 7.5 V		[46]
Ag-based ORR catalysts					
C.-Y. Wu et al.	Ag/CNC	Standard[a]	j = 200 mA cm^{-2} at E = 0.8 V (30% KOH, T = 25 °C). Galvanostatic discharge on Ag/CNC at j = 200 mA cm^{-2} with a moderate performance decrease after 80 h		[60]
Y. Yang et al.	Ag on Ni foam	Standard[a]	Insignificant voltage deterioration during 120 h galvanostatic discharge at T = 40 °C		[61]
H. Meng et al.	AgW_2C/C	Standard[a]	Test on RRDE in 1 M KOH, 25 °C: j = 6 mA cm^{-2} at 200 mV (Hg/HgO). For comparison: j = 4.5 for Ag/C, j = 5.8 for Pt/C.	Microwave intermittent heating method (IMH)	[64]

Gillette Corp. (USA)	$AgMnO_4$ + 5–10% MnO_2 + C + PTFE	GDL: 30–70% PTFE	3 electrode cell test $AgMnO_4$ + 5% MnO_2—0.16 V (SHE) at 28 mA cm^{-2}, $AgMnO_4$ + 10% MnO_2 at 50 mA cm^{-2}	MnO_2 forms by heating $Mn(NO_3)_2$.	[66]
		Catalyst layer: 10–30% PTFE	LSV shows the limiting current, 51 mA cm^{-2}, was achieved at −0.25 V vs. Hg/HgO or 1.1 V vs. Zn.	Dual Catalyst $AgMnO_4$ prepared by reducing silver permanganate	
Luz Electric Fuel Izrael Ltd.	Raney silver catalyst + PTFE = 5:1 (wt.%) (24 mg cm^{-2})	Blocking layer (air side) carbon + PTFE (6–10 mg cm^{-2}) pressed onto Ni mesh or foam	After 5 h of discharge the cell showed a peak current of 10 A at 0.9 V (200 mA cm^{-2} peak current at the air cathode)		[67]
Zinc Air Power Corp.	Ag_2O + 10% $LaNiO_3$	Standard[a]	No degradation during 500 h in 32% KOH		[68]
Alupower, Inc. (USA	5% Ag + 15% BP2000 + 10% Daxad + 60% Teflon RPM T-30	Impregnated layers and fine nickel mesh precoated with an adhesive were passed through an oven		Daxad was an additive to increase silver adsorption on carbon black	[48]
CoTMPP-based ORR catalysts					
Ovonic Battery Company, Inc. (Rochester, USA)	1. 50% (20% CoTMPP/C) + 50% (15% CoO_x + 5% MnO_x/C) 2. 2.5% MnO_x + 7.5% CoO_x/C	Standard[a]	j = 120 mA cm^{-2} at voltage 0.1 V for 2.5% MnO_x + 7.5% CoO_x/C and, 50% CoTMPP + 50% (15% CoO_x + 5% MnO_x)	1. Mix NH_4OH + carbon 2. Add Co (Mn) SO_4 3. Mix 1 and 2 4. Add NaOH 5. Washing 5. Filtration 6. Dry at 80 °C	[71]
Reves, Inc. (USA)	1. 4% CoTMPP + 15% BP2000 + 60% Teflon RTM T-30 2. MnO_2 and/or $AgNO_3$ (Pt, Co_3O_4)	Standard[a]	j = 500 mA cm^{-2} (wet coating) and 200 mA cm^{-2} (dry powder process) at 1 V discharge in KOH	1. Single roll pressing with impregnation: CoTMPP + H_2O + PTFE 2. Sinter 200–350 °C 3. Laminating porous Teflon sheets at nip pressure 100 lb $in.^{-1}$ at T = 250–350 °C Note: sintering of the impregnated polymer binder into pores of the foamed support	[77]
Lutz Electric Fuel Cell Israel Ltd.	10% CoTMPP/C + Nafion + FEP + FEP-coated PTFE fibers	Standard[a]	E = −0.29 V (Hg/HgO) at j = 0.4 A cm^{-2}, stable during 200 h test. Electrode was soaked overnight in 7 M KOH at 25 °C and duty cycled for 1 h (20 s—200 mA cm^{-2}, 45 s—50 mA cm^{-2}, 45 s—0 mA cm^{-2})	Co-precipitation	[78]
Power zinc Electric (China)	CoTMPP + MnO_x/C	Standard[a]	1. j = 500 mA cm^{-2} at E = −0.498 V (Hg/HgO) in 1 M KOH at T = 25 °C (half-cell) 2. j = 216 mA cm^{-2} at E = 1 V in 30% KOH (ZAFC)		[88]
Nitride-based ORR catalysts					
N. Miura et al.	60% Mn_4N/C + PTFE	Standard[a]	At −125 mV (Hg/HgO) or 0.8 V (RHE) performance was stable at j = 2400 mA cm^{-2} for 5 h, at j = 300 mA cm^{-2} for 50 h in 9 M NaOH, at 80 °C	Co-precipitation	[97]
Spinel-based ORR catalyst					
W.J. King et al.	$NiCo_2O_4$ spinel	Standard[a]	0.87 V in 5 M KOH and room temperature	Pyrolysis of the metal salts	[99]

Table 14 (*Continued*)

Assignee	Catalyst composition	Air cathode design	Performance	Catalyst fabrication method	Reference
E. Rios et al.	$Mn_xCo_{3-x}O_4$ + PTFE ($0 < x < 1$) spinel	Standard[a]	RRDE at 2500 rpm $j = 100\ mA\ cm^{-2}$ at $E = 0.2$ in 1 M KOH at $T = 25\ ^\circ C$	Pyrolysis of the metal nitrites	[100]
Perovskite-based ORR catalysts					
T. Hyodo et al.	Perovskites		Performance, $mA\ cm^{-2}$ at −160 mV (Hg/HgO)		[111]
	$LaMnO_3$		1266		
	$LaCoO_3$		1006		
	$LaNiO_3$		468		
	$LaCrO_3$		344		
	$LaFeO_3$		273		
	$La_{0.8}Sr_{0.2}FeO_3$		519		
	$La_{0.6}Sr_{0.4}Fe_{0.6}Co_{0.4}O_3$		682		
	$La_{0.6}Sr_{0.4}Fe_{0.6}Mn_{0.4}O_3$		922		
M. Hayashi et al.	$LaNiO_3$		$j = 300\ mA\ cm^{-2}$ at $E = -80$ mV (Hg/HgO) for 140 h in 8 M KOH at 60 °C	Reverse micelle	[114]
A.C. Tseung et al.	$LaCoSrO_3$		$j = 2\ mA\ cm^{-2}$ at 500 mV (DHE) in 45% KOH at room temperature		[116]
Pyrochlore-based ORR catalysts					
A. Gibeney et al.	$Pb_2M_{2-x}Pb_xO_{7-}$		$j = 6 \times 10^{-3}$ at −100 mV (Hg/HgO) in 1 M NaOH at 25 °C		[134]
Metal hydroxide-based ORR catalyst					
High-Density Energy Inc. (USA)	Ni, Co, Fe hydroxide + carbon black + PTFE	Standard[a]	No data		[127]
Pt-based catalyst					
Gould Inc. (USA)	Ag + Pt + MnO_2 + C + PTFE	Standard[a]	No data		[128]
G. Henry et al.	10% Pt/C	Standard[a]	Cell voltage of 0.69 V in 6 M KOH at $T = 50\ ^\circ C$		[129]
Bifunctional electrodes					
Westinghouse Electric Corp.	Iron–air fuel cell similar to ZAFC) with alkaline electrolyte:	1. Hydrophillic layer $CuS0_4$, $NiWO_4$, WC + 20% Co or WS_2 + WC	Test of WC + Ag + C + PTFE + FEP after duty cycle (16 h charge at 25 $mA\ cm^{-2}$ and 8 h discharge at 25 $mA\ cm^{-2}$) at −0.3 V (Hg/HgO). Initial $j = 100\ mA\ cm^{-2}$, $j = 40\ mA\ cm^{-2}$ after 934 h. Stable performance during first 750 h, voltage drop 50 mV at 25 $mA\ cm^{-2}$		[131]
	1. $CuS0_4$, $NiWO_4$, WC + 20% Co 2. WS_2 + WC or WC + 1–20% Co 3. WS + C + PTFE 4. WC + Ag + C + PTFE (FEP)	2. Hydrophobic layer—FEP sheet			
Westighouse Electric Corp.	30 parts Ag + 30 parts WC (coated with 12% Co) + 32 parts PTFE + 90 parts carbon black	Catalyst impregnated into 45–95% of collector's pores	half-cell test (Ni counter electrode): no deterioration in performance during 134 charging cycles in KOH		[132]
Westighouse Electric Corp.	3% (5–10%) Ag (ORR) + ∼[7% (10–15% $FeWO_4$) + 7% (10–15%) WC + ∼12% (10–15%) Co (OER] + ∼54% C] + ∼22% PTFE, Ag loading—2 $mg\ cm^{-2}$	1st layer—GDL: EC-600JD + PTFE 2nd layer: current collector impregnated with low SA carbon black + ORR catalyst + PTFE 3rd layer: catalyst + Low SA carbon black + High SA carbon black + PTFE	No data	Reduction of $AgNO_3$ with hydrazine	[133]
C-T. Liu et al	[ORR—Ag] + [OER—$CoWO_4$ + WC + WS_2 + NiS + 10–15% Co] + 20% PTFE	Standard[a]			[136]

AER Energy Resources, Inc.	ORR catalyst [(0.3–2%)CoTMMP + (4–10%)$LaNi_{1-x}Co_x$ + (1–4%)Ag + (18–32%)Co_xO_y + OER catalyst [(1–20%)WC + (1–20%)Co + (1–7%)$FeWO_4$ + (1–7%)NiS] + AB-50 + PTFE	1. $E_{1\ OER}$ for ORR catalyst > $E_{2\ OER}$ of OER catalyst 2. ORR catalyst concentration on the electrolyte side > ORR concentration on the air side 3. OER catalyst concentration on the electrolyte side < OER concentration on the air side			[137]
Revolt Technologies AS (Norvey)	1. Catalyst layer: 63.5% XC500 + 15% PTFE + 13% $MnSO_4$ + 8.5% La_2O_3 2. 15% PTFE + 69% XC500 + 8% MnO_2 + 8% La_2O_3 3. 58% XC500 + 15% PTFE + 19% $AgNO_3$ + 8% $MnSO_4$ 4. GDL: 65% C + 35% PTFE	Standard[a]	Current densities (mA cm^{-2}) at E = 1 V vs. Zn in 6.6 M KOH (three-electrode cell) for the electrodes: 13% $MnSO_4$ + 8% La_2O_3 (270), La_2O_3 (280), $MnSO_4$ (80)	Co-precipitation	[138]
Zinc Air Power Corporation	OER electrode 30% Ag + 70% $LaNiO_3$	The single functional electrode and third electrode are separated.	Charge/discharge capacity is stable for tricell designed ZAFCs (40 cycles) in 32% KOH	Co-precipitation	[140]
Y. Shmizu et al.	$La_{1-x}A_xFe_{1-y}Mn_yO_3$ (A = Sr, Ca)		J = 200–300 mA cm^{-2} at E = −300 mV (Hg/HgO) in 7 M KOH, 25 °C, air flow		[143]
Y. Shimizu et al.	$La_{0.6}Ca_{0.4}Co_{0.8}Fe_{0.2}O_3$		j = 200 mA cm^{-2} at E = −150 (Hg/HgO) in 1 M NaOH at 25 °C		[145]

[a] Standard ZAFC design: Teflon film (air side) + current collector + gas diffusion layer + catalyst layer.

4.8. Pyrochlore

The lead ruthenate pyrochlore ($Pb_2Ru_2O_{6.5}$) effectively promotes the four-electron ORR pathway and can be used as a self-supported catalyst to avoid oxidation of the carbon-support materials.

4.9. Comparisons

A comparison of the ORR catalysts developed for ZAFCs shows that electrodes based on Ag, FeTMPP, Mn_4N, spinel $Mn_xCo_{3-x}O_4$ [100], manganese nitride Mn_4N [97], and lead ruthenate pyrochlore ($Pb_2Ru_2O_{6.5}$) [126] promote the four-electron ORR pathway and have the highest ORR activity. However, the catalysts with the best durability in concentrated KOH electrolyte have been based on MnO_2 [29–34], $LaMnO_3$ [111], $LaCoO_3$ [111] and $LaNiO_3$ [112], each of which demonstrated a higher durability than Pt. Additional improvement in the durability of $LaNiO_3$ have been achieved by coating the catalyst with electronically conductive polypyrrole (PPy) [101].

4.10. Bifunctional electrodes for secondary ZAFC

Liu et al. [133] developed a complicated bifunctional ZAFC electrode design, composed of [3% Ag (ORR)] + [7% $FeWO_4$ + 7%(88% WC + 12% Co) + 7% NiS (OER)] + 22% PTFE + 54% carbon black (low and high BET surface areas). The details of the composition are:

- The ORR takes place on the carbon.
- Hydrated cobalt oxide promotes decomposition of the ORR by-product hydroxides.
- Silver is a more active ORR catalyst than Co.
- Silver, in the presence of cobalt and nickel, has improved ORR activity.
- Silver, in the presence of NiS, reacts to form Ag_2S, which is relatively stable in alkaline electrolyte.
- WC and Ni–Fe hydrated oxides (the latter formed during the charging process) determine the relatively high OER activity.

4.11. Design of the air cathode

It has been demonstrated that the standard design of an air cathode, consisting of a Teflon film on the air side, a current collector, a gas diffusion layer, and a catalyst layer, could be significantly improved by:

- Combining carbon blacks with low (AB-50) and high (EC-600JD) surface areas in the GDL, for better water management (a 30:70 ratio).
- Combining PWA and EC-600JD with a 60:40 ratio in the catalyst layer.
- Utilizing different Teflon concentrations in the GDL (30–70%) and catalyst layers (10–30%).
- Utilizing different concentrations of catalysts in the air and electrolyte sides of the electrode.
- Combining two different hydrophobic compounds (PTFE/FEP) [127,129] (Table 14).

5. Summary

1. Analysis of the air cathode market for primary alkaline ZAFCs showed that the eight main types of ORR catalysts are based on MnO_x, CoO_x-MnO_x, Ag, CoTMPP/FeTMPP, metal nitrides, spinel, perovskites, and pyrochlore compositions. Note that the separation of the effects of catalyst composition, cell design and

air cathode structure (carbon black concentrations and ratios, binding agent concentration, etc.) on ZAFC performance is very difficult, so it is difficult to compare the performance of ZAFCs with different catalysts and test conditions.

2. MnO_x-based catalysts have MnO_2 concentrations in the range of 5–30%. MnO_2 is characterized by the two-electron ORR pathway, a high activity for peroxide decomposition and sufficient stability in concentrated alkaline solution. The performance of these cathodes depends strongly on the method of fabrication. Rayovac Corp. (USA) developed a stable MnO_2-based cathode with a voltage 1.15 V at 150 mA cm^{-2} (during a 15 h durability test in 30% KOH).
3. Ag promotes, in contrast with MnO_x, the direct four-electron ORR pathway, and also has high ORR activity and high stability in alkaline solution. Ag is the cheapest precious metal ($17 per troy oz.). The most effective Ag-based catalysts consist of Ag/C, Ag + MnO_2, AgO-$LaNiO_3$, and (Ag + W_2C = 1:1)/C. The performance of the basic catalyst Ag/C (BET 333 m^2 g^{-1}, 15–30 nm particle sizes) on CNC is j = 200 mA cm^{-2} at 0.99 V. The other Ag-based catalyst (Ag:W_2C = 1:1) has higher ORR activity than Ag/C in 1 M KOH. This catalyst could be used in the bifunctional electrode as Ag is active for ORR and WC is active for both OER and ORR in alkaline solution.
4. The cobalt oxide, Co_3O_4, is more active for ORR than MnO_2 but is less stable in alkaline solution (Co_2O_3 is more stable than Co_3O_4). The catalyst 2.5–5% MnO_x + 5–7.5% CoO_x combines the advantages of both of these oxides with a performance of j = 120 mA cm^{-2} at −0.1 V, T = 25 °C. NiO has higher stability and ORR activity than Co_3O_4 and it should be evaluated as a replacement for MnO_2 in the combined catalysts.
5. CoTMPP and FeTMPP correspondingly promote the two- and four-electron ORR pathways and have high and low stability in alkali, respectively. The composite catalyst CoTMPP-FeTMPP/C combines the advantages of both compounds. The more stable CoTMPP was also modified with the addition of MnO_x, MnO_x + CoO_x, Ag, etc. CoTMPP with Ag was used as the ORR catalyst in a bifunctional catalyst developed by ReVolt Technolgy Inc. CoTMPP was synthesized from $CoCO_3$ and TMPP precursors with a 2 h heat treatment at 800 °C in inert gas. Another ZAFC producer, Powerzinc Electric Inc. (China), developed CoTMPP + MnO_2 catalyst with a high performance of j = 216 mA cm^{-2} at 1.0 V in 30% KOH and T = 25 °C.
6. The 60% Mn_4N/C catalyst promotes the direct four-electron ORR pathway and demonstrated stable performance over 50 h: j = 300 mA cm^{-2} at −125 mV (Hg/HgO), T = 80 °C in 9 M NaOH. Other metal nitrides such as CrN, Mn_4N, Fe_2N, Co_3N, and Ni_3N yield to Mn_4N in ORR activity.
7. Spinel-based catalysts, such as $NiCo_2O_4$, $Mn_xCo_{3-x}O_4$ ($0 < x < 1$), and $CoFe_2O_4$, have higher ORR activity than the separate CoO_x, MnO_x, and NiO-based catalysts. The performance of a ZAFC with a $NiCo_2O_4$ + PTFE air cathode in 5 M KOH at room temperature is j = 200 mA cm^{-2} at −0.87 V. Mn strongly inhibits the oxidation of OH^- ions in contrast with Co_3O_4, which has ORR active surface ions observable in $Mn_xCo_{3-x}O_4$ catalyst ($0 < x < 1$). Its performance of j = 100 mA cm^{-2} at 0.2 V is low in comparison with $NiCo_2O_4$. The additional improvement of spinel-based catalyst stability in alkaline solution is achieved by the electrodeposition of polypyrrole (PPy) polymer film on an example catalyst, $Ni_{0.3}Co_{2.7}O_4$) + PPY/C.
8. The pyrochlore-based catalysts, such as $Pb_2Ru_2O_{6.5}$, promote the desirable four-electron ORR pathway and can be used as self-supported catalysts, which avoids oxidation of the carbon-support materials. However, their stability may not be high enough during extended operation, as the precious metal ruthenium is not stable in concentrated alkaline solution.
9. The perovskite-based ORR catalysts, such as $LaMnO_3$ and $LaCoO_3$, have high ORR activity, but Co-based perovskite is not stable enough in alkaline solution. The Co-free perovskite catalysts such as $La_{0.6}Sr_{0.4}Fe_{0.6}Mn_{0.4}O_3$ are more stable and can be used in bifunctional electrodes as well. The latter catalyst demonstrates significantly improved stability as a ZAFC air cathode: j = 500 mA cm^{-2} at −260 mV (Hg/HgO) for 70 h. Other promising perovskite compositions, $La_{0.6}Ca_{0.4}Co_{0.8}B_{0.2}O_3$ (B = Mn, Fe, Co, Ni, Cu), promote the two-electron ORR pathway at high currents and the four-electron pathway at low currents. $La_{0.6}Ca_{0.4}Co_{0.8}Fe_{0.2}O_3$ has one of the highest BET surface areas (28 m^2 g^{-1}) and HO_2^- decomposition rates of the perovskite-based catalysts.
10. The bifunctional electrodes for secondary rechargeable ZAFCs provide a higher energy density than Li-ion batteries. They have very complicated multilayer designs and compositions, which can include 5–10 components. Several companies have patented bifunctional electrodes, but all of them have insufficient ORR catalyst lifetimes at the high OER potential (~2.1 V). Westinghouse, Diamond Shemrock, and ReVolt Technology Inc. are companies that have successfully developed commercial bifunctional electrodes. The ORR catalysts are based on Ag (with NiS stabilizer), CoTMPP, or $LaNiO_3$ and the OER catalysts are based on WC, WS, $FeWO_4$, $NiWO_4$, etc.

References

[1] K. Kinoshita, Electrochemical Oxygen Technology, John Wiley & Sons Inc., New York, 1992.
[2] D.-Q. Yang, Y.-Q. Yang, US Patent 7,264,898 (2007).
[3] G. Woodroff, R.A. Putt, US Patent 5,328,778 (1994).
[4] J.F. Cooper, US Patent 5,434,020 (1995).
[5] D. Sieminski, Recent Advances in Rechargeable Zinc–Air Battery Technology, 12th Annual Battery Conference on Applications and Advances, January, 1997, p. p171.
[6] S.F. Bender, J.W. Cretzmeyer, T.F. Reise, in: D. Linden (Ed.), Handbook of Batteries, McGraw-Hill, Inc., New York, 1995, p. 13.1.
[7] J.W. Cretzmeyer, Commercial Zinc–Air Batteries, Power Sources, Academic Press, 1977, p. 269.
[8] F.M. Harris, M.J. Schimpf, Proceedings of the Annual Battery Conference, 1994, p. 146.
[9] E.M. Morse, Zinc–Oxygen Battery System, 19th Annual Power Sources Conference, 1965, p. 109.
[10] R.A. Putt, G. Woodruff, Proceedings of the Intersociety Energy Conversion Engineering Conference 1, 1993, p. 1085.
[11] R.A. Powers, Advances and Trends in Primary and Small Secondary Batteries, IEEE AES Syst. Mag. (1994) 32.
[12] M. Schimpf, Rechargeable Zinc Air Batteries Market and Technology Overview, Multidimensional Digital Filters, Technical Conference, Session 1, March, 1995, pp. 30–36.
[13] M. Schroeder, Hearing Instrum. 38 (1987) 11.
[14] D. Linden, T.B. Reddy, Handbook of Batteries, 3rd edition, McGraw-Hill Professional, 2001.
[15] Rechargeable Batteries Applications Handbook, Gates Energy Products, Newnes, 1997.
[16] Website of Power Air Corp.: www.poweraircorp.com.
[17] Y. Harats, B. Koretz, J.R. Goldstein, M. Korall, Batterien und Batterriemanagement Conference, Essen, Germany, February 22–23, 1995.
[18] Website of Frost & Sullivan: www.frost.com.
[19] J.R. Goldstein, B. Koretz, Proceedings of the 28th Intersociety Energy Conversation Engineer Paper #N93410, Atlanta, GA, 1993.
[20] N. Naimer, B. Koretz, R. Putt, Website of Electric Fuel, Zinc–Air Batteries for UAV and MAVs, 2002.
[21] Website of Powerzinc Electric Inc. (China): www.powerzinc.com/en.
[22] G.S. Moy, J.E. Oltman, R.B. Dopp, J.L. Passaniti, M.A. Ward, US Patent 6,461,761 (2002).
[23] W.W. Clark, E. Poolucci, J. Cooper, J. Cleaner Prod. 11/4 (2003) 427.
[24] E. Yeager, J. Mol. Catal. 38 (1986) 5.
[25] S.B. Kanungo, K.M. Parida, B.R. Sant, Electrochim. Acta 26 (1981) 1157.
[26] S. Liompart, L.T. Yu, J.C. Mas, A. Mendiboure, R. Vignaud, J. Electrochem. Soc. 137 (1990) 371.
[27] J.P. Brenet, J. Power Sources 4 (1979) 183.
[28] L. Mao, T. Sotomura, K. Nakatsu, K. Nobuharu, D. Zhang, T. Ohsaka, J. Electrochem. Soc. 149 (2002) A504.
[29] G.A. Deborski, US Patent 4,256,545 (1978).
[30] W.A Armstrong, US Patent 3,948,684 (1976).
[31] J. Passaniti, R.B. Dopp, US Patent 5,378,562 (1995).
[32] J.L. Passaniti, R.B. Dopp, US Patent 5,308,711 (1994).

[33] S. Bach, N. Baffier, M. Henry, J. Livage, FR Patent 2,659,075 (1991).
[34] W.H. Hoge, US Patent 4,906,535 (1988).
[35] W.H. Hoge, US Patent 5,032,473 (1991).
[36] R.B. Dopp, US Patent 5,656,395 (1997).
[37] N. Golovin, US Patent 6,444,609 (2002).
[38] N. Golovin, US Patent 6,428,931 (2002).
[39] R. Ndzebet, US Patent 6,780,347 (2002).
[40] N. Koshiba, H. Hayakawa, K. Momose, A. Ohta, US Patent 4,595,643 (1984).
[41] R.L. Sassa, D. Zuckerbrod, W. Buerger, J.E. Bacino, US Patent 6,921,606 (2005).
[42] F. Sun, F. Wang, US Patent 6,248,476 (2001).
[43] L. Borbelly, F. Wang, US Patent 6,248,476 (1990).
[44] J.J. McEvoy, US Patent 4,585,710 (1986).
[45] G.S. Kelsey, P.Chalilpoyil, P.D. Trainer, A. Kaplan, G. Cintra, V.H. Vu, J.D. Sillesky, US Patent 6,207,322 (1998).
[46] I. Roche, E. Chainet, M. Chatenet, J. Vondrak, J. Phys. Chem. C 111 (2007) 1434.
[47] I. Roche, E. Chainet, M. Chatenet, J. Vondrak, J. Appl. Electrochem. 38 (2008) 1195.
[48] J. Vondrak, J.B. Klapste, J. Velicka, M. Sedlarikova, J. Reiter, I. Roche, E. Chainet, J.F. Fauvarque, M. Chatenet, J. New Mater. Electrochem. Syst. 8 (2005) 209.
[49] P. Zoltowski, D.M. Drazic, L. Vorkapic, J. Appl. Electrochem. 3 (1973) 27.
[50] P. Bezdicka, T. Grygar, B. Klapste, J. Vondrak, Electrochim. Acta 45 (1999) 913.
[51] B. Klapste, J. Vondrak, J. Velicka, Electrochim. Acta 47 (2002) 2365.
[52] J. Vondrak, B. Klapste, J. Velicka, M. Sedlarikova, R. Cerny, J. Solid State Electrochem. 8 (2003) 44.
[53] J. Vondrak, B. Klapste, J. Velicka, M. Sedlarikova, V. Novak, J. Reiter, J. New Mater. Electrochem. Syst. 8 (2005) 1.
[54] J. Vondrak, M. Sedlarikova, V. Novak, J. New Mater. Electrochem. Syst. 1 (1998) 25.
[55] E.A. Ticianelli, F.H.B. Lima, F.M. Calegaro, 209th ECS Spring Meeting, Denver, CO, May 7–12, 2006.
[56] J. Yang, J.J. Xi, Electrochem. Commun. 5 (2003) 306.
[57] K. Matsuki, H. Kamada, Electrochim. Acta 31 (1986) 13.
[58] D. Sepa, M. Vojnovic, A. Damjanovic, Electrochim. Acta 15 (1970) 1355.
[59] F.H.B. Lima, C.D. Sanches, E.A. Ticianelli, J. Electrochem. Soc. 152 (2005) A1466.
[60] C.-Y. Wu, P.-W. Wu, P. Lin, Y.-Y. Li, Y.-M. Lin, J. Electrochem. Soc. 154 (2007) B1059.
[61] Y. Yang, Y. Zhou, J. Electroanal. Chem. 397 (1995) 271.
[62] K. Kinoshita, Carbon, John Wiley & Sons Inc., New York, 1988.
[63] C.-C. Chang, T.-C. Wen, Mater. Chem. Phys. 47 (1997) 203.
[64] H. Meng, P.K. Shen, Electrochem. Commun. 8 (2006) 588.
[65] K. Hohne, K. Mund, US Patent 3,94,0510 (1973).
[66] E. Curelop, S. Lu, S. McDevitt, J. Sunstrom, US Patent 6,632,557 (1999).
[67] J. Goldstein, N. Naimer, E. Khasin, A.Brokman, US Patent 5,190,833 (1993).
[68] Z. Zhong, US Patent 6,383,675 (2002).
[69] R. Bhaskara, US Patent 5,053,375 (1990).
[70] E. Ndzebet, US Patent 2003146414 (2001).
[71] S.R. Ovshinsky, C. Fierro, B. Reichman, W. Mays, J. Strebe, M.A. Fetcenko, A. Zallen, T. Hicks, US Patent 7,097,933 (2003).
[72] M. Maya, C. Oreccia, M. Strano, P. Tosco, M. Vanni, Electrochim. Acta 46 (2000) 423.
[73] C. Mocci, S. Trassatti, J. Mol. Catal. A: Chem. 204–205 (2003) 713.
[74] X.-Y. Xie, Z.-F. Ma, X.-X. Ma, Q. Ren, V.M. Schmidt, L. Huang, J. Electrochem. Soc. 154 (2007) B733.
[75] C. Mocci, A.C. Tavares, S. Trassati, P. Tosco, M. Manzoli, F. Boccuzzi, in: E.W. Boomam, C.M. Doyle, C. Cominellis, J. Winnick (Eds.), Energy and Electrochemical Processes for a Cleaner Environment, vol. 2001–2023, The electrochemical Society, Pennington, NJ, 2001, p. 363.
[76] S.Lj. Gojkovic, S. Gupta, R.F. Savinell, J. Electrochem. Soc. 145 (1998) 3493.
[77] W. Yao, T. Tsai, US Patent 6,368,751 (2002).
[78] N. Naimer, E.E. Khasin, J.R. Goldstein, J. Sassen, US Patent 5,242,765 (1993).
[79] R. Jiang, L. Xu, R. Jin, S. Dong, Fenxi Huaxue 13 (1985) 270.
[80] L. Zhang, J. Zhang, D.P. Wilkinson, H. Wang, J. Power Sources 156 (2006) 171.
[81] D. Chu, R. Jiang, Solid State Ionics 148 (2002) 591.
[82] N. Oyama, F.C. Anson, Anal. Chem. 52 (1980) 1192.
[83] J.P. Collman, P. Denisevich, Y. Konai, M. Marocco, C. Koval, J. Am. Chem. Soc. 102 (1980) 6027.
[84] M. Lefevre, J.P. Dodelet, P. Bertrand, J. Phys. Chem. B 104 (2000) 11238.
[85] F.C. Anson, J. Am. Chem. Soc. 102 (1980) 6027.
[86] H. Jahnke, M. Schonborn, G. Zimmermann, Top. Curr. Chem. 61 (1976) 133.
[87] S.Lj. Gojkovic, S. Gupta, R.F. Savinell, J. Electroanal. Chem. 462 (1999) 63.
[88] X.Y. Xie, Z.F. Ma, X.X. Ma, Q. Ren, V.M. Schmidt, L. Huang, J. Electrochem. Soc. 154 (2007) B733.
[89] I. Iliev, S. Gamburzev, A. Kaisheva, J. Power Sources 17 (1986) 345.
[90] S. Gambuzev, A. Kaisheva, I. Iliev, 29th ISE Meeting, Budapest, Hungary, August 28–September 2, 1978, p. 106, Ext. Abst., Part II.
[91] R.J. van Veen, C. Visser, Electrochim. Acta 24 (1979) 221.
[92] V.S. Bagotsky, M.R. Tarasevich, K.A. Radyushkina, O.A. Levina, S.I. Andruseva, J. Power Sources 2 (1977/1978) 333.
[93] K. Wiesener, A. Fuhrmann, Z. Phys. Chem. 261 (1980) 411.
[94] Y. Kiros, Int. J. Electrochem. Sci. 2 (2007) 285.
[95] F. Solomon, Y. Genodman, J. Irizarry, US Patent 4,877,694 (1989).
[96] J.H. Zagal, F. Bedioui, J.P. Dodelet, N_4-Macrocyclic Metal Complexes, Springer, New York, 2006.
[97] N. Miura, H. Horiuchi, Y. Shimitzu, N. Yamazoe, Nippon Kagaku Kaishi (1987) 671.
[98] A.C.C. Tseung, S. Jasem, Electrochim. Acta 22 (1977) 31.
[99] W.J. King, A.C. Tseung, Electrochim. Acta 19 (1974) 485.
[100] E. Rios, J.L. Gautier, G. Poillerat, P. Chartier, Electrochim. Acta 44 (1998) 1491.
[101] J.L. Gautier, J.F. Marco, M. Gracia, J.R. Gancedo, V. de la Garza Guadarrama, H. Nguyen, P. Chartier, Electrochim. Acta 48 (2002) 119.
[102] H. Nguyen, V. de la Garza Guadarrama, J.L. Gautier, P. Cartier, Electrocihim. Acta 8 (2003) 2389.
[103] R.N. Singh, B. Lal, M. Malviya, Electrochim. Acta 49 (2004) 4605.
[104] N. Miura, Y. Shimizu, N. Yamazoe, T. Seiyama, Nippon Kagaku Kaishi (1985) 644.
[105] N. Miura, Y. Shimizu, N. Yamazoe, Nippon Kagaku Kaishi (1986) 751.
[106] Y. Shimizu, K. Uemura, H. Matsuda, N. Miura, N. Yamazoe, J. Electrochem. Soc. 137 (1990) 3430.
[107] T. Hyodo, Y. Shimizu, N. Miura, N. Yamazoe, Denki Kagaku Kogyo Butsuri Kakagku 62 (1984) 158.
[108] T. Hyodo, N. Miura, N. Yamazoe, Mater. Res. Soc. Sump. Proc. 393 (1995) 79.
[109] T. Hyodo, M. Hayashi, N. Miura, N. Yamazoe, J. Electrochem. Soc. 143 (1996) L266.
[110] T. Hyodo, M. Hayashi, S. Mitsutake, N. Miura, N. Yamazoe, J. Appl. Electrochem. 27 (1997) 745.
[111] T. Hyodo, Y. Shimizu, N. Miura, N. Yamazoe, Denki Kagaku (1993) 158.
[112] Y. Matumoto, H. Yoneyama, H. Tamura, Chem. Lett. (1975) 661.
[113] J. Lamminen, J. Kivisaari, M.J. Lampinen, M. Viitanen, J. Vuorisalo, J. Electrochem. Soc. 138 (1991) 905.
[114] M. Hayashi, H. Uemura, K. Shimanoe, N. Miura, N. Yamazoe, Electrochem. Solid-State Lett. 1 (1998) 268.
[115] Y. Masayoshi, S. Kengo, T. Yasutake, Y. Noboru, Catal. Today 126 (2007) 313.
[116] A.C. Tseung, H.L. Bevan, J. Electroanal. Chem. Interfacial Electrochem. 45 (1973) 429.
[117] T. Kudo, H. Obayshi, M. Yoshide, J. Electrochem. Soc. 124 (1977) 321.
[118] T. Kudo, H. Obayshi, T. Gejo, J. Electrochem. Soc. 122 (1975) 159.
[119] X. Wang, P.J. Sebastian, M.A. Smit, H. Yang, S.A. Camboa, J. Power Sources 124 (2003) 278.
[120] J. Ponce, J.-L. Rehspringer, G. Poillerat, J.L. Gautier, Electrochim. Acta 46 (2001) 3373.
[121] R.N. Singh, B. Lal, Int. J. Hydrogen Energy 27 (2002) 45.
[122] S.K. Tiwari, P. Chartier, R.N. Singh, J. Chem. Soc. Faraday Trans. 91 (1995) 187.
[123] H. Arai, S. Muller, O. Haas, J. Electrochem. Soc. 147 (2000) 3587.
[124] K.L.K. Yeung, A.C. Tseung, J. Electrohem. Soc. 125 (1978) 878.
[125] J.B. Goodenough, R. Manoharan, M. Paranthaman, J. Am. Chem. Soc. 112 (1990) 2076.
[126] J. Prakash, D. Tryk, E. Yeager, J. Power Sources 29 (1990) 413.
[127] Y-K. Shun, C-L. Lou, US Patent 6,127,061 (2000).
[128] A.P.O. Blanchart, C.J. E. Van Der Poorten, US Patent 4,696,872 (1987).
[129] G. Henry, US Patent 4,333,993 (1982).
[130] B.G. Demczyk, C.T. Liu, J. Electrochem. Soc. 129 (1982) 1159.
[131] E.S. Buzzet, US Patent 3,977,901 (1976).
[132] J. Chottiner, US Patent 4,152,489 (1979).
[133] C-T. Liu, J.F. Jackovitz, US Patent 5,318,862 (1994).
[134] A. Gibeney, D. Zuckerbrod, in: J. Thomson (Ed.), Power Source, Academic, New York, 1983.
[135] D. Tryk, W. Alfred, E. Yeager, First report for the period October 9, 1980 to April 1, 1983, prepared by Western Reserve University. Subcontract 1377901 for Lawrence Livermore National Laboratory, Livermore, CA.
[136] C-T. Liu, B. Demczyk, US Patent 4,444,852 (1984).
[137] V.R. Shepard, Y.G. Smalley, R.D.Bentz, US Patent 5,306,579 (1994).
[138] B. Trugve, US Patent 20071666602A1 (2007).
[139] J. Coetzer, M.M. Thackeray, US Patent 4,288,506 (1981).
[140] Z. Zhimin, US Patent 6,383,675 (2002).
[141] Y. Shimizu, H. Matsude, A. Nemoto, N. Miura, N. Yamazoe, Prog. Batteries Battery Mater. 12 (1993) 108.
[142] A.N. Jain, S.K. Tiwari, R.N. Singh, P. Chartier, J. Chem. Soc: Faraday Trans. 91 (1995) 1871.
[143] T. Hyodo, T. Shmizu, N. Miura, N. Yamazoe, Denki Kagaku 62 (1994) 158.
[144] Y. Shimizu, A. Nemoto, T. Hyodo, N. Miura, N. Yamazoe, Denki Kagaku 61 (1993) 1458.
[145] Y. Shimizu, H. Matsuda, N. Miura, N. Yamazoe, Chem. Lett. (1992) 1033.
[146] T. Lippert, M.J. Montenegro, M. Dobeli, A. Weidenkaff, S. Muller, P.R. Willmott, A. Wokaun, Prog. Solid State Chem. 35 (2007) 221.
[147] S.-W. Eom, C.-W. Lee, M.-S. Yun, Y.-K. Sun, Electrochim. Acta 52 (2006) 1592.
[148] S. Muller, F. Holzer, H. Arai, O. Haas, J. New Mater. Electrochem. Syst. 2 (1999) 227.
[149] G.Q. Zhang, X.G. Zhang, Electrochim. Acta 49 (2004) 873.
[150] F. Angerer, N. Tomov, EP Patent 0082553 (1983).
[151] Website of London Metal Exchange: www.lme.co.uk.